Mon. Not. R. Astron. Soc. **000**, 1–?? (2007) Printed 5 November 2007 (MN LATEX style file v2.2)

The Arecibo Galaxy Environment Survey: II. A HI view of the Abell cluster 1367 and its outskirts.

L. Cortese[1], R. F. Minchin[2], R. R. Auld[1], J. I. Davies[1], B. Catinella[2,3], E. Momjian[2], J. L. Rosenberg[4], R. Taylor[1], G. Gavazzi[5], K. O'Neil[6], M. Baes[7], A. Boselli[8], G. Bothun[9], B. Koribalski[10], S. Schneider[11], W. van Driel[12]

[1] *School of Physics and Astronomy, Cardiff University, Cardiff CF24 3AA, UK*
[2] *NAIC-Arecibo Observatory, HC3 Box 53995, Arecibo, PR 00612, USA*
[3] *Max-Planck-Institut für Astrophysik, D-85748 Garching, Germany.*
[4] *Harvard-Smithsonian Centre for Astrophysics, 60 Garden Street, MS 65, Cambridge, MA 02138-1516, USA*
[5] *Universitá degli Studi di Milano-Bicocca, Piazza della Scienza 3, 20126 Milano, Italy*
[6] *National Radio Astronomy Observatory, Green Bank, WV 24944, USA*
[7] *Sterrenkundig Observatorium, Universiteit Gent, Krijgslaan 281 S9, B-900 Gent, Belgium*
[8] *Laboratoire d'Astrophysique de Marseille, BP8, Traverse du Siphon, F-13376 Marseille, France*
[9] *Physics Department, University of Oregon, 1371 East 13th Avenue, Eugene, OR 97403, USA*
[10] *Australia Telescope National Facility, CSIRO, Epping, NSW, Australia*
[11] *Department of Astronomy, University of Massachusetts, Amherst, MA 01003, USA*
[12] *Observatoire de Meudon, 5 Place Jules Janssen, 92195 Meudon, France*

Accepted 2007 October 28. Received 2007 October 1; in original form 2007 August 10

ABSTRACT

We present 21 cm HI line observations of 5×1 square degrees centered on the local Abell cluster 1367 obtained as part of the Arecibo Galaxy Environment Survey. One hundred sources are detected (79 new HI measurements and 50 new redshifts), more than half belonging to the cluster core and its infalling region. Combining the HI data with SDSS optical imaging we show that our HI selected sample follows scaling relations similar to the ones usually observed in optically selected samples. Interestingly all galaxies in our sample appear to have nearly the same baryon fraction independently of their size, surface brightness and luminosity. The most striking difference between HI and optically selected samples resides in their large scale distribution: whereas optical and X-ray observations trace the cluster core very well, in HI there is almost no evidence of the presence of the cluster. Some implications on the determination of the cluster luminosity function and HI distribution for samples selected at different wavelength are also discussed.

Key words: surveys – galaxies:clusters:individual:(A1367) – galaxies:evolution – galaxies:peculiar – radio lines:galaxies

1 INTRODUCTION

With the advent of wide field surveys our knowledge of galaxy properties has significantly improved. The large amount of high quality data of nearby and high redshift objects obtained so far is allowing astronomers to shed light on how galaxies formed and evolved at different redshifts and in different environments (e.g. Cowie et al. 1996; Gavazzi et al. 1996; Kauffmann et al. 2003). However our picture of the Universe still remains limited since it is mostly based on the study of rest-frame optical selected objects. First of all optically-selected galaxies already contain, by definition, a large amount of stars which may not be the case in younger or less evolved galaxies. Secondly, surface brightness selection is very dramatic and nearly all catalogued objects lie in an extremely narrow range of surface brightnesses (Freeman 1970).

Since each wavelength has its own selection effects and traces different baryonic components, the combination of blind surveys at various frequencies is of vital importance. Alternative methods of baryon selection will allow us to have a less biased view of our Universe and enable us to correctly reconstruct the evolutionary history of galaxies (e.g. Buat et al. 2007). In particular, the most interesting results can come from the comparison of optical surveys with blind surveys tracing components not directly related to stellar

emission like, for example, neutral and molecular hydrogen. For molecular hydrogen we will have to wait a couple of years for the first results from ALMA, but with the advent of multi-beam instruments on large single dish radio telescopes it has become possible during the last decade to carry out fully sampled blind HI surveys of the sky (e.g. Rosenberg & Schneider 2000; Henning et al. 2000; Barnes et al. 2001; Lang et al. 2003; Minchin et al. 2003; Davies et al. 2004). Neutral hydrogen is extremely important because it represents the fuel for the future star formation activity of a galaxy. It is also one of the galactic components that can most easily be affected by environmental mechanism (e.g. ram pressure, tidal interaction) influencing its star formation history. Therefore HI line observations of galaxies can provide us with some of the most powerful diagnostics on the role of the environment in regulating the evolution of galaxies (Haynes & Giovanelli 1984; Giovanelli & Haynes 1985). What we lack is deep and high spatial resolution HI blind surveys of cluster of galaxies and their outskirts. The HI Parkes all Sky Survey (HIPASS) has represented a real breakthrough for HI blind surveys, but its low spatial resolution ($\sim$15 arcmin) has made it very difficult to carry out detailed studies of high density regions. Fortunately, with the refurbishing of the 305m Arecibo radio telescope, blind HI surveys with much improved sensitivity, spatial (3.5 arcmin beam^{-1}) and velocity (5 km s^{-1}) resolution have become possible thanks to the installation of the ALFA multi beam instrument.

The Abell cluster 1367, due to its proximity (z$\sim$0.0216, V$\sim$6500 km s^{-1}) and to the fact that it is currently forming at the intersection of two filaments in the Great Wall (Cortese et al. 2004), represents an ideal target for HI surveys (e.g. Sullivan et al. 1981; Chincarini et al. 1983; Gavazzi 1987; Solanes et al. 2001; Gavazzi et al. 2006). It is ideal for the study of the properties of HI selected galaxies and environmental effects. For these reasons, Abell 1367 is one of the region observed as a part of the Arecibo Galaxy Environment Survey (AGES, Auld et al. 2006), one of the new HI blind survey carried out with the ALFA multi-beam system[1]. AGES aims to study the atomic hydrogen properties of different galactic environments to faint sensitivity limits; low HI masses (6×10^8 M$_\odot$, assuming a 200 km s^{-1}velocity width at 92.8 Mpc, the distance of the A1367 cluster) and column densities of $\sim 3\times10^{18}$ cm^2 (for a source that fills the beam). The environments AGES will survey range from apparent voids in the large-scale structure of galaxies, via isolated spiral galaxies and their haloes, to galaxy-rich regions associated with galaxy clusters and filamentary structures. AGES plans to cover 5×4 square degrees centered on Abell 1367. Here we report on the early results obtained from observations of a subset of the whole AGES-A1367 region: a 5×1 square degree area centered on the cluster core.

[1] The other three main extragalactic ALFA surveys are ALFALFA (Giovanelli et al. 2005), AUDS (Freudling et al. 2005) and ZOA (Henning et al. 2006).

2 AGES OBSERVATIONS AND DATA REDUCTION

As part of the AGES, we observed the Abell 1367 region in May 2006 and April 2007 using the ALFA feed array at the 305-m Arecibo Telescope. A total of $\sim$63 hours observing time were allocated with an average observing time of $\sim$2.3 hours per night. Since the allocated time was insufficient to cover all the AGES-A1367 region (5×4 square degrees) we decided to give the highest priority to the cluster center and its immediate outskirts covering a strip of $\sim$5×1 square degrees (11:34:00<R.A.(J.2000)<11:54:15, 19:15<Dec(J.2000)<20:20) centered on the cluster core. The observation and data reduction techniques adopted by AGES are extensively described in Auld et al. (2006); here we will only provide a brief summary of them.
AGES uses the 7-feed ALFA multi-beam receiver and a spectral line backend capable of instantaneously recording spectra from the two linear polarizations of each beam and covering a bandwidth of 100 MHz. The angular resolution is given by the size of the ALFA beams ($\sim$3.3×3.8 arcmin) and the velocity resolution is $\sim$25kHz, corresponding to $\sim$ 5.5 km s^{-1}. Observations are performed in *drift scan mode* (e.g. Giovanelli et al. 2005): the array is kept at a fixed azimuth and elevation while the sky drifts overhead. The Earth's rotation rate governs the on source time in a drift scan. For Arecibo this means that each point in the sky takes $\sim$12 s to cross the beam. Twenty-five separate scans are then required to reach the 300 s/beam integration time. In order to compensate for the change in parallactic angle, and thus achieve uniform sky coverage, ALFA must be rotated before every scan and, in order to attain fully sampled sky coverage, it is necessary to stagger the declination (Dec.) of individual scans by $\sim$1 arcmin (half the beam separation). We record data every second and total power values for each of the seven beams, both polarizations and 4096 channels, are recorded as four-bit floating point numbers. Calibration is performed at the beginning of every scan using a high-temperature noise diode that is injected into each beam for a duration of 1 s. A uniform final depth of $\sim$ 300 sec was achieved for all of the area observed.

Data reduction was performed using the AIPS++ packages LIVEDATA and GRIDZILLA (Barnes et al. 2001), developed by the Australian Telescope National Facility (ATNF). LIVEDATA performs bandpass estimation and removal, Doppler tracking and calibrates the residual spectrum. GRIDZILLA is a gridding package that co-adds all the spectra using a suitable algorithm, to produce 3D data cubes. The Abell 1367 5×1 square degrees region was gridded using a median gridding technique into 1×1 square arcmin pixels, each of which contains a 4096 channel spectrum, and was smoothed at a velocity resolution of 10 km s^{-1}. The AGES observing strategy is highly successful at reducing sidelobe variations by making a Nyquist-sampled map with every ALFA beam individually. Thus, when the observations are median combined, the variations across the beams are removed, leaving a circular beam with symmetrical sidelobes at a $\sim$5-10% level (Minchin et al. 2007). The output data cube has two spatial dimensions and the spectral dimension can be chosen by the user to be frequency, wavelength or velocity. The noise distribution is fairly gaussian with a standard deviation of 0.8439$\pm$0.0003 mJy, consistent with

the expected value (Auld et al. 2006) for minimal smoothing of the beam. The cube is publicly available and can be downloaded at the following link $http://www.naic.edu/\sim ages/public\_data.html$.

2.1 Data contamination: Radio frequency interference, the Milky Way and 3C264.

Radio frequency interference (RFI) represents a constant source of contamination in certain regions of the observed spectral window. In particular two main RFI sources were present in all the scans: the San Juan FAA radar at 1350 MHz and its 3rd harmonic at 1387.8 MHz. In addition an intermittent source of RFI (GPS satellite L3) appeared only in some of the scans at approximately 1381 MHz. The strong constant sources at 1350 MHz (V$\sim$14620$\pm$140 km s^{-1}) and 1387.8 MHz (V$\sim$7009$\pm$19 km s^{-1}) completely obscure a part of the cosmic volume: in particular the 1387.8 MHz RFI lies approximately at the velocity of Abell 1367 making part of the cluster volume inaccessible. The intermittent GPS source at 1381 MHz (V$\sim$8500 km s^{-1}) reduces our sensitivity limit and could significantly influence the number of sources detected in a frequency range $\sim$ 300 km s^{-1}wide.

In addition to the RFI another two sources of contamination affect our data. The first one is the Galaxy: LIVEDATA is not able to correctly subtract the strong emission from the Milky Way, resulting in a blindness of our survey in about the velocity range -50$< V <$+50 km s^{-1}. Moreover the Abell 1367 region includes the 3C264 radio galaxy (R.A.=11:45:05.5, Dec=+19:36:23). This strong radio source has a 1.4GHz continuum flux of $\sim$5 Jy, producing strong spectral standing waves and making a $\sim$4 arcmin radius region around the galaxy inaccessible.

2.2 Source Extraction

In every blind survey a crucial step in the data reduction is represented by the source extraction. The objective is to obtain a catalogue of confirmed sources to well defined selection limits: as the signal-to-noise ratio (S/N) decreases, the contamination by spurious noise signals quickly rises. Detection techniques need to be optimized to discriminate real from spurious signals as well as possible.

Currently source extraction is carried out using three different methods: the cube is visually inspected independently by two of us (in this case RRA and LC) and by an automatic extractor (Polyfind, written by R. F. Minchin) based on a peak flux threshold. The automatic extractor is essentially based on the cross-correlation with templates method described by Davies et al. (2001). The program initially looks for peak values above a pre-defined value (in this case 4σ) and then cross-correlates with templates accepting the best fit as long as the correlation coefficient is above 0.75 and the total signal-to-noise ratio of the detection is above 4 (Davies et al. 2004). Automatically extracted candidates are then checked 'by eye', visually inspecting the full AGES spectrum summed from a 5$\times$5 arcmin^2 box around the position of the detection. The aim of this process is to quickly remove obvious spurious detections while not rejecting any real source. These methods provided a list of 104 candidate HI sources[2], of which 78 were detected by all the three different signal extraction techniques. In the following we will refer to these 78 objects as "sure" sources and to the remaining 26 as "possible" sources.

The distribution of the total 21 cm flux as a function of the line width at the 50% level of peak maximum for our 104 candidate sources is shown in Fig.1. Filled circles indicate "sure" sources while empty circles are "possible" sources. The void in the bottom right part of the plot (i.e. large velocity widths and small fluxes) is due to a selection effect present in the source extraction technique: at fixed low total flux it is easier to detect a narrow HI source, since the survey is not flux but surface brightness limited. In order to compare the AGES S/N threshold with the recent results presented by ALFALFA (Giovanelli et al. 2007) we plotted in Fig.1 a S/N limit of S/N_{tot}=6.5 for our survey, where (Saintonge 2007):

$$S/N_{tot} = \frac{1000 \times F_{tot}}{W_{50}} \times \frac{w^{1/2}}{rms} \quad (1)$$

F_{tot} is the total flux in Jy km s^{-1}, W_{50} is the velocity width measured at the 50% level, w is either $W_{50}/(2 \times \Delta V)$ for $W_{50} < 400$ km s^{-1}or $400/(2 \times \Delta V)$ for $W_{50} \geqslant 400$ km s^{-1}, ΔV is the spectral velocity resolution and rms is the r.m.s. noise across the spectrum measured in mJy at $res.$ spectral resolution. In our case $res.$=10 km s^{-1}. The great majority of our "sure" sources lie well above S/N_{tot}=6.5 while the "possible" sources have $S/N_{tot} \approx$6.5, in agreement with Saintonge (2007). This suggests that also for our sample S/N_{tot}=6.5 is a reliable threshold for discriminating between "sure" and "possible" sources.

3 L-WIDE RADIO FOLLOW-UP OBSERVATIONS

In order to test the reliability of our extraction technique and the real nature of the 26 "possible" sources, 10 hours of telescope time where scheduled with the Arecibo single pixel L-band wide (LBW) receiver in April 2007. The LBW observations were made covering a spectral band of 12.5 MHz (2048 spectral channels) centered at the expected source recessional velocity. The integration time varied between 5 and 10 minutes depending on the intensity of the source, reaching an rms in the range $\sim$0.5-0.8 mJy beam^{-1} at a velocity resolution of 10 km s^{-1}. All observations were taken using the position-switching technique, with each blank sky (or OFF) position observed for the same duration, and over the same portion of the telescope dish (Az and El) as the on-source (ON) observation. Each 5 min + 5 min ON + OFF pair was followed by a 10 s ON + OFF observation of a calibrated noise diode. None of the 26 observed sources lies within the sidelobes of a "sure" HI detection, making unlikely a sidelobe contamination of the L-Wide follow-up observations. Of the 26 "possible" sources, only 4 (indicated with crosses in Fig.1) were not confirmed by Arecibo follow-up observations. We therefore have a sample of 100 sure HI sources

[2] Here we do not include two extended High Velocity Cloud complexes extending over a great part of the observed region at 140$< V <$ 210 km s^{-1}. These systems are described in the Appendix of this paper.

detected in the 5×1 square degrees observed by AGES in the Abell 1367 region.

4 SOURCE CATALOGUES

All the 100 sources in the sample were inspected and parametrized using the MIRIAD task MBSPECT (Sault et al. 1995). The source position was estimated from a Gaussian fit to the moment map within the galaxy velocity range and the spectrum was then extracted from the data cubes. This spectrum is a weighted average, with the weight depending on the distance of each pixel from the fitted position. Velocity widths were then measured at the 20% and 50% levels (W_{20} and W_{50}) relative to the peak signal, using a width-maximizing algorithm (Lewis 1983). The uncertainties in each derived quantity are computed following the recipes given by Koribalski et al. (2004). In Table 1 we present the main parameters of all the 100 HI sources detected in the cube, namely:
Col.1: HI source ID
Col.2-3: HI R.A. (J.2000) coordinate and relative error
Col.4-5: HI Dec. (J.2000) coordinate and relative error
Col.6: Heliocentric velocity and relative error (cz, i.e. optical reference frame), measured as the midpoint between the velocities where the flux density reaches 50% of peak maximum level.
Col.7: Velocity width and relative error of the source line profile measured at the 50% level of peak maximum.
The velocity widths are not corrected for instrumental broadening, turbulent motions, disk inclination or cosmological effects.
Col.8: Velocity width and relative error of the source line profile measured at the 20% level.
Col.9: Peak Flux density and relative error in mJy.
Col.10: Total Flux and relative error in Jy km s^{-1}.
Col.11: Object flag, defined as follows: Flag 0 indicates sources detected by all the three independent methods used for source extraction making them reliable sources. Flag 1 indicates objects confirmed only after Lwide follow-up observations. Flag 2 indicates objects which are contaminated by RFI: they are in general sure detections but the HI parameters (e.g. flux, velocity width, etc.) can be strongly affected and should not be used.
The AGES source catalogue and the spectra for all the HI sources are publicly available at the following link *http* : *//www.naic.edu/* $\sim$ *ages/public_data.html*.

The results of the LBW follow-up observations are presented in Table 2, which lists the following:
Col.1: HI source ID
Col.2: Heliocentric velocity and relative error of the source (cz), measured as the midpoint between the channels at which the flux density drops to 50%.
Col.3: Velocity width and relative error of the source line profile measured at the 50% level.
The velocity widths are not corrected for instrumental broadening, turbulent motions, disk inclination or cosmological effects.
Col.4: Velocity width and relative error of the source line profile measured at the 20% level.
Col.5: Total Flux and relative error in Jy km s^{-1}.
Col.6: The rms noise per channel at 10 km s^{-1} velocity resolution.
In Fig.2 we compare the measurements obtained using the ALFA and L-wide receivers for the 22 sources confirmed during follow-up observations (filled circles). Although these are the lowest S/N sources within our sample, the agreement between the dataset is quite good with an average dispersion of 19 km s^{-1}in recessional velocity, 35 km s^{-1}in velocity width and $\sim$14% in total flux.

4.1 Comparison with previous works

The Coma-A1367 supercluster is one of the regions most intensively investigated by optically selected HI surveys (i.e. Haynes et al. 1997; Gavazzi et al. 2006). However only 21 out of the 100 sources detected by AGES had a previous HI measurement. The high number of new HI detections in AGES ($\sim$79%) confirms once more the importance of HI blind surveys for having an unbiased view of the neutral hydrogen distribution in the local Universe. Among the 21 sources previously known (Gavazzi 1989; Haynes et al. 1997; Springob et al. 2005b; Gavazzi et al. 2006), three of these objects (namely CGCG97-079, CGCG97-087 and CGCG127-052) are strongly contaminated by RFIs in the AGES cube, and cannot be used for a comparison with the literature. Our measurements for the remaining 18 objects are in satisfactory agreement with past works as illustrated in Fig.2 (empty circles). There is quite a good agreement in both fluxes and velocity width measurements and the average scatter is $\sim$10% in flux and $\sim$ 28 km s^{-1}in velocity width. In one case (CGCG97-138) our velocity width estimate differs considerably from literature values: Gavazzi (1989) gives a velocity width of 160 km s^{-1}whereas we measure only 62 km s^{-1}). However our new L-wide measurement is consistent with the value obtained from the AGES cube (W=58 km s^{-1}).

4.2 Optical Counterparts

The Abell 1367 region has been covered in the optical by the Sloan Digital Sky Survey (SDSS) as part of Data Release 5. We have used this homogenous dataset to look for optical counterparts of our HI sources. We cross-correlated our list of HI detections with the SDSS galaxy catalogue using a search radius of 4 arcmin. In the few cases in which no candidate optical counterpart was found, we visually inspected the SDSS plates to look for low surface brightness galaxies not included in the SDSS catalogue. Once a candidate optical counterpart was found, we looked into the literature and NED for an estimate of its optical recessional velocity. In addition for 5 of the 46 candidates without an available redshift in the literature we obtained new optical recessional velocity estimates in January-Febrary 2007 using the imaging spectrograph BFOSC attached to the Cassini 1.5 m telescope at Loiano (Italy). Observations and data reduction techniques applied are described in Cortese et al. (2003).

Confirmed optical counterparts are defined as those optical galaxies lying within 4 arcmin and having a recessional velocity within $\pm$200 km s^{-1}from the radio velocity. Candidate optical counterparts are galaxies which lie within 4 arcmin but do not have a published optical recessional velocity. Of the 100 HI sources in our sample, 55 have confirmed

optical counterparts, 34 have a unique candidate (i.e. no optical recessional velocity available) optical counterpart, 7 have two or more candidate counterparts and 4 sources appear to have no optical counterparts. Three of these objects are associated with the interacting groups in the outskirts of Abell 1367 described in the Appendix of this paper. A list of the optical counterparts (confirmed and candidate) associated with the HI sources is presented in Table 3.

In Fig.3 we show the distribution of the difference between the optical and HI positions and recessional velocities for the 55 sources having confirmed optical counterparts. Optical and radio measurements show a very good agreement with a median offset of only 18 arcsec in position (consistent with the typical error of 16 arcsec in the estimate of the centroid for radio sources) and of $\sim$4$\pm$16 km s^{-1}in recessional velocity.

For all the HI sources having 1 optical counterpart (confirmed or candidate) we downloaded SDSS-DR5 *ugriz* images (Adelman-McCarthy et al. 2007) and performed aperture photometry and surface brightness profile decomposition using the task *ellipse* within IRAF. The radial profiles have been constructed by integrating the available images within elliptical, concentric annuli. The ellipticity and position angles have been determined and then fixed using the i band image. Total magnitudes, effective radii (r_e) and effective surface brightness (μ_e, i.e. average surface brightness within r_e) have been determined following the procedure of Gavazzi et al. (2000).

4.3 Comparison with other HI-blind surveys

Fig.4 illustrates the sky (upper panel) and the HI mass vs distance distributions (lower panel) for all the 100 sources detected in the A1367 cube. Over half of the sources (54) belongs to the Abell 1367 cluster and its outskirts, lying in the velocity range 4000$<$ V $<$9000 km s^{-1}. This roughly explains why in this cube we detect twice the number of sources than in other AGES fields: excluding the Abell 1367 region (4000$<$ V $<$9000) we are left with 46 sources consistent with the number found in NGC628 (Auld et al. 2006), NGC1156 (Auld et al. in prep.) and NGC7332 (Minchin et al. 2006). The bottom panel of Fig.4 allows a direct comparison of AGES with ALFALFA (Giovanelli et al. 2005) showing that, in the same area of sky, ALFALFA would miss $\sim$ half of the sources detected here. This is quite expected since ALFALFA has an integration time $\sim$ 6.3 times shorter ($\sim$48 sec instead of $\sim$300 sec) than AGES. More impressive is the difference between AGES and the northern HIPASS extension (Wong et al. 2006): whereas AGES finds 100 sources, HIPASS does not detect a single galaxy in the 5$\times$1 square degrees here studied.

5 PHYSICAL PROPERTIES OF THE AGES-A1367 SAMPLE

We use the HI data from AGES and the optical data from SDSS to derive the physical properties of our sample. The HI mass ($M(HI)$) is defined as:

$$M(HI) = 2.36 \times 10^5 D^2 F_{tot} \qquad (M_\odot) \qquad (2)$$

where F_{tot} is the integrated HI flux in Jy km s^{-1}and D is the galaxy distance in Mpc. For those galaxies belonging to Abell 1367 (4000$<$ V $<$9000 km s^{-1}) we assume D=92.8 Mpc (Sakai et al. 2000) while we assume $D = V/H_0$ with $H_0 = 70$ km s^{-1}Mpc^{-1} for the rest of the sample. The stellar mass is obtained from the optical colors and luminosity as defined in (Bell et al. 2003b):

$$log(M_{star}) = -0.222+0.864(g-r)+\frac{M(i)-4.56}{-2.5} \qquad (M_\odot) \qquad (3)$$

where $M(i)$ is the absolute magnitude in the i band. Therefore the total amount of baryons is M_{bar}=M_{star}+$M(HI)$ (e.g. Bell et al. 2003a). This quantity does not include the contribution of helium and metals (usually assumed equal to 1.4$\times$M(HI)), the molecular hydrogen and any warm or hot gas component. Therefore M_{bar} must be considered as a lower limit of the real value. Finally we define the galaxy dynamical mass as:

$$M_{dyn} = \gamma \frac{R_{75} \times W_c^2}{2G} \qquad (4)$$

where G is the gravitational constant, R_{75} is the radius containing 75% of the i band flux, W_c is the HI velocity width (here we use the average between W_{50} and W_{20} HI velocity widths) corrected for inclination and γ is the ratio between R_{75} and the extension of the HI emission (i.e. $\gamma = R_{HI}/R_{75}$). γ should lie between 2-3 (Salpeter & Hoffman 1996; Swaters et al. 2002), but for our galaxies radio interferometric data (necessary to estimate R_{HI}) is not available, so this remains unknown and we leave it as a free parameter. The galaxy inclination is obtained from the ellipticity determined in the i band via:

$$cos(i)^2 = \frac{(1-e)^2 - q_0^2}{1-q_0^2} \qquad (5)$$

where e is the galaxy ellipticity and q_0 is the intrinsic axial ratio of the galaxy here assumed equal to 0.13 (Giovanelli et al. 1997). We excluded from this analysis face-on galaxies having $e < 0.1$ (20 galaxies), for which it is not possible to accurately estimate the dynamical mass.

The correlations between different optical and HI quantities and their distributions for our sample are presented in Fig.5. From left to right: the ratio of the gas to stellar mass, the baryon fraction (M_{bar}/M_{dyn}), the total HI mass, the effective surface brightness in i band, the $g-i$ color and the dynamical mass are presented. Only galaxies with one optical counterpart and $e < 0.1$ (69 galaxies) are shown: filled dots are objects with confirmed optical counterparts while empty dots indicate objects with optical counterpart candidates. Our sample covers almost three orders of magnitude in both HI and dynamical mass. The optical surface brightness distribution shows a significant tail at low surface brightness ($\mu(i)_e$ $\sim$22.5-24 mag arcsec^{-2}) as usually observed in HI selected sample (e.g. Spitzak & Schneider 1998). HI selected samples are often considered as composed of only blue, gas-rich galaxies. This is not the case for our sample which spans over 1 magnitude in the $g-i$ color, as is typically observed in optically selected samples (Baldry et al. 2004), and covers a wide range of gas to stars ratios (M_{gas}/M_{star}): from gas poor objects ($M_{gas}/M_{star} \sim 0.1$) to extremely gas rich galaxies ($M_{gas}/M_{star} \sim 10$). More massive galaxies appear to be redder, have higher surface brightness and lower gas content than dwarf systems. This is also

found to be the case in optically selected samples (Gavazzi et al. 1996). Well known relations like color-mass, surface brightness-mass and hydrogen-dynamical mass are here rediscovered. Unfortunately the small number of objects in our sample does not allow a more detailed comparison between the slopes, scatters and distributions of the relations followed by HI and optically selected galaxies. We postpone this kind of analysis to the moment when we will have a significantly large AGES database at our disposition.
The most intriguing result presented in Fig.5 is the absence of any correlation involving the baryon fraction. On the contrary all galaxies in our sample appear to have almost the same baryon fraction $< log(M_{bar}/M_{dyn}) >$=(-0.2-log(γ))$\pm$0.13 independently from their mass, surface brightness or gas content. The little dispersion in the baryon fraction distribution is in fact well within the observational errors. Assuming 0.1 dex error in the HI mass (see Sec.4.1), in the stellar mass (Bell et al. 2003b) and in the dynamical mass, the uncertainty on the estimate of the baryon fraction is $\sim$0.17 dex. The gas and stellar mass fraction cover a larger dynamical range (i.e. have a larger dispersion: $< log(M_{star}/M_{dyn}) >$=(-0.4-log($\gamma$))$\pm$0.24 and $< log(M(HI)/M_{dyn}) >$=(-0.6-log(γ))$\pm$0.3)) than the baryon fraction, as shown in Fig.6 and accordingly to the Kolmogorov-Smirnov test the baryon fraction distribution is not compatible with the gas and star fraction distributions at a 99.99% confidence level.

We can therefore conclude that our sample shows approximately the same baryon fraction. A constant baryonic mass fraction in galaxies implies a direct correlation between dynamical mass and baryonic mass: exactly what is usually required for the Tully-Fisher relation (McGaugh & de Blok 1998; McGaugh et al. 2000). This result is also consistent with the recent study of an optically selected sample of extremely low mass dwarf galaxies carried out by Geha et al. (2006). To our knowledge, this is the first confirmation of a constant baryonic fraction coming from an HI selected sample. This observational evidence is also consistent with models of galaxy formation (Bullock et al. 2001; Crain et al. 2007) but in contradiction with recent models of galaxy evolution which invoke supernova feedback and other physical mechanisms to remove baryons preferentially from low mass systems and to reproduce the observed scaling relations (Cole et al. 2000; Governato et al. 2007). Even if our sample includes low surface brightness galaxies it appears that physical mechanisms that preferentially remove baryons from low mass galaxies are not effective in the mass range and selection criteria of our sample. We remark that the only way to obtain a correlation between the baryon fraction and the dynamical mass in our sample would be to assume that γ (i.e. the ratio of the HI to optical radius) is a strong function of the mass and/or the contribution of molecular hydrogen, hot and warm gas to the total baryon mass varies with the mass of the galaxy. We cannot a priori exclude the first possibility, even if unlikely since Cayatte et al. (1994) found that the ratio of the HI to optical radius varies by only 20% along the Hubble sequence. Conversely, the molecular hydrogen represents only $\sim$15% of the total gas reservoir in normal, late-type galaxies (Boselli et al. 2002) and the contribution of hot and warm gas components is a few percents ($\leqslant$1-2%) of the total gas mass (e.g. Tschöke et al. 2001; Higdon et al. 2006) making the second scenario extremely unlikely.

6 COMPARING THE OPTICAL AND HI VIEW OF THE ABELL CLUSTER 1367

More than half of the HI sources detected in the cube belong to the Abell 1367 volume. This includes not only the cluster core but also a part of the Great Wall: a large scale filament of galaxies connecting Abell 1367 to the Coma cluster (Zabludoff et al. 1993). All galaxies in the filament lie approximately at the same distance from us as Abell 1367, implying that the system A1367+Great Wall constitutes a volume limited sample. At the distance of Abell 1367 ($\sim$92.8 Mpc) the surveyed sky area has a physical size of 8.1$\times$1.6 Mpc^{-2} and our sensitivity limit for a source with W_{50}=200 km s^{-1}is $\sim$6$\times$10^8 M$_\odot$. Since the virial radius of Abell 1367 is $\sim$ 2.3 Mpc (Girardi et al. 1998), our region covers the cluster virialized region and its immediate neighborhood.

In order to compare the HI and optical properties of the Abell 1367 region we extracted an optically selected sample of galaxies from SDSS-DR5. We select all galaxies in the AGES region having $g < 17$ mag (corresponding to $L_g > 2 \times 10^9$ L$_\odot$ at the Abell 1367 distance): 259 galaxies in total, of which 208 have optical redshift available and 155 are confirmed cluster members (4000$< V <$9000 km s^{-1}).

We note that the time necessary to carry out a HI targeted survey of this optically selected sample (reaching the same AGES noise level) would be similar to the observing time needed by AGES to cover all the 5$\times$1 square degrees in Abell 1367.

6.1 Sky distribution

The sky distribution of the 54 HI sources belonging to the A1367 region (4000$< V <$9000 km s^{-1}) is shown in Fig.7. It is interesting to note that no significant over-density of sources is observed corresponding to the cluster center: the only HI galaxy lying well within the X-ray cluster contours belongs to a small group of galaxies infalling for the first time into the cluster, suggesting that it is just entering the cluster and it is only projected on the center of Abell 1367 (Cortese et al. 2006). This appears much more evident when we compare the sky distribution of our sample with the typical sky distribution obtained for the optically selected sample. In Fig.7 we show the distribution of the 155 confirmed cluster members (empty circles) and of the 51 galaxies without redshift available[3] (empty stars) extracted from the optically selected sample.

The optical selected sample is strongly clustered on the cluster center and almost half of the sources detected lie within the X-ray emitting region. Moreover the "Finger of God" feature, typical of clusters of galaxies, is not observed in the HI selected sample (see Fig.8). Conversely the HI-selected galaxies show a different pattern in the wedge diagram shown in Fig.8: galaxies on the east side of the cluster have a lower recessional velocity than galaxies in the west side. This probably suggests the presence of two different infalling directions into the cluster core as proposed by Cortese et al. (2004).

The differences observed between the optically and HI

[3] The majority of galaxies without redshift have a magnitude $g <$ 16.5 mag, suggesting that a not negligible fraction is composed by background galaxies (Cortese et al. 2004).

selected samples are somehow expected since clusters of galaxies are made HI deficient structures through the combination of the morphology-density relation (Dressler 1980; Whitmore et al. 1993) and of the "gas-density" relation (Giovanelli & Haynes 1985; Gavazzi et al. 2006). This is also consistent with recent determinations of the correlation function for HI selected samples (Meyer et al. 2007; Basilakos et al. 2007) which show that HI galaxies are among the least clustered objects in the Universe.

The influence of the harsh cluster environment is barely visible when we look for radial variations of the gas to star mass ratio and of the HI-deficiency (see Fig.9). The HI deficiency is defined as the difference, in logarithmic units, between the observed HI mass and the value expected from an isolated galaxy with the same morphological type T and optical linear diameter D: HI DEF $= < \log M_{HI}(T^{obs}, D^{obs}_{opt}) > -logM^{obs}_{HI}$ (Haynes & Giovanelli 1984). We used the equations in Solanes et al. (1996) to calculate the expected HI mass from the optical diameter. The HI deficiency does not significant vary with the cluster-centric distance (Fig.9, bottom panel), contrary to what usually observed in optically selected samples (i.e. Haynes & Giovanelli 1984; Solanes et al. 2001; Gavazzi et al. 2006). A slight decrease on the average value of the gas to star mass ratio is observed in correspondence of the cluster center, however also in this case no strong gradients have been found. We can therefore conclude that when observed in HI the Abell cluster 1367 almost completely disappears and the only evidence of its hidden presence is a slightly higher number of galaxies with a low gas to star mass ratio near the cluster core.

6.2 The HI mass distribution and optical luminosity function.

The Abell 1367 local volume can be used for a more detailed analysis of selection effects representing a unique dataset for which complete samples independently selected at optical and radio wavelengths are available. We are particularly interested in the comparison of the HI mass distribution and optical luminosity function estimated from the two samples. In the past, different authors have used optically selected samples to determine the HI mass distributions of galaxies in the local Universe obtaining results significantly different from radio selected samples (Briggs & Rao 1993; Springob et al. 2005a; Gavazzi et al. 2005). We therefore used the optically selected sample extracted from SDSS-DR5, complete to $g < 17$ mag, in order to compare the HI distribution and the g band luminosity function for optically and HI selected galaxies.

Contrary to the HI selected sample, the SDSS sample is not complete in redshift, but the redshift completeness rapidly drops below 50% for $g \sim 16.5$ mag ($\sim 3 \times 10^9$ L$_\odot$). This complicates the estimate of the luminosity function at low luminosities. In order to overcome the redshift incompleteness of cluster samples we used the *completeness corrected* method proposed by De Propris et al. (2003). This method is based on the assumption that the spectroscopic sample (i.e. galaxies with redshift available) is 'representative' of the entire cluster, i.e. the fraction of galaxies that are cluster members is the same in the (incomplete) spectroscopic sample as in the (complete) photometric one.

The HI mass distributions obtained from the optically and HI selected samples are shown in Fig.10. As expected the two samples produce HI distributions significantly different. The optical selected sample drops quicker at low HI masses and does not include nearly half of the HI sources in the A1367 volume. The two samples start to differ at $M(HI) \sim 2\times10^9$ M$_\odot$, well before our sensitivity limit. Low luminosity, low surface brightness, gas rich objects are in fact not included in the optical sample, but they represent a significant fraction of the total HI budget in Abell 1367. This result is consistent with the recent work by Springob et al. (2005a) who showed that the faint end slope of the HI mass function for an optically selected sample is less steep than the one obtained from a 21 cm selected sample. Our analysis suggests that this difference is mainly due to selection effects and that HI distributions obtained from optically selected samples cannot be generally considered as good proxies of the HI mass function in the local Universe.

The HI and optically selected samples also differ in the estimate of the optical luminosity functions (Fig.11, lower panel). The luminosity function (LF) for the HI selected galaxies is flatter and includes fewer objects (i.e. lower Φ^*) than the one obtained from the optically selected sample. A great part of this difference is due to the overabundance of red ($g - i > 0.9$), gas poor galaxies in the center of Abell 1367: more than 80% of bright red galaxies ($L > 10^9$ L$_\odot$) in the A1367 region are not detected at 21 cm (see Fig.11, upper panel). The difference between the two samples is less evident if we compare the luminosity functions obtained only for blue galaxies (Fig.11, middle panel), but even in this case the HI sample misses $\sim$30% of blue cluster galaxies.

This result is quite interesting since we generally associate HI deficiency to red colors. In order to further investigate the properties of these blue galaxies not detected in HI, in Fig.12 we compare the color $g - i$, i magnitude relation for the confirmed cluster members in the optically (empty circles) and HI selected (triangles) samples. Almost all the HI galaxies lie on the blue sequence, but the opposite is not true: not all the galaxies in the blue sequence are detected in HI. This could be due to a number of different reasons. First of all we have to take into account our sensitivity limit ($M(HI) \sim 6\times10^8$ M$_\odot$ for W$_{50} \sim 200$ km s^{-1}) which we need to relate to optical color and magnitude. To do so we have used the correlation between the HI mass and i band luminosity ratio and the $g-i$ color observed for our sample. The best bisector linear fitting gives the following relation:

$$g - i = (-0.61 \pm 0.05) \times \log\left(\frac{M(HI)}{L(i)}\right) + (0.57 \pm 0.04) \quad (6)$$

with a dispersion of 0.37 dex. We can use this equation to estimate our sensitivity limit, which is indicated by the solid line in Fig.12. We consider undetected blue galaxies those objects not detected by AGES, lying outside the one σ region and with a $g - i$ color bluer than 0.9 mag: 10 galaxies in total. Some of these sources lie within (in both space and velocity) strong HI galaxies and can be missed, due to the size of the Arecibo beam (FWHM$\sim$3.5 arcmin) and to the fact that in these cases the HI emission is totally assigned to the bright source. Moreover some galaxies have a recessional velocity within the RFIs frequencies and cannot be detected. Excluding these cases (indicated with crosses in Fig.12, Left) we are left with eight blue galaxies which are not detected in HI. These objects have a g band luminosity

in the range $2\times10^9 < L_g < 10^{10}$ L$_\odot$ (i.e. -19.4< $M(g)$ <-17.9 mag), implying that we are dealing with intermediate mass galaxies and not dwarf systems. Moreover their broadband morphology and structural parameters are indistinguishable from the other blue HI detected galaxies. The limits obtained from Eq.6 imply that the undetected galaxies have a HI deficiency $\geqslant$0.37, suggesting that we are dealing with blue, deficient objects, consistent with the marginal detection of two of these galaxies (CGCG97-092, CGCG97-093) by deeper surveys (Gavazzi et al. 2006) implying an HI deficiency 0.31 and 0.57 respectively. This suggests that we are dealing with the same population of HI poor, star forming spirals originally observed in nearby clusters by Kennicutt et al. (1984). Only when observed in Hα[4] these galaxies appear different from healthy spirals, showing a truncation of the star forming disk. In particular, in all but one object for which Hα data are available (8 galaxies, Iglesias-Páramo et al. 2002) the Hα radius (e.g. the isophotal radius within $10^{-16.5}$ ergs cm^{-2} s^{-1} Å^{-1} arcsec^{-2}) is $\sim$2-4 times less extended than the r band 24th mag arcsec^{-2} isophotal radius (see Table 4). This is consistent with various independent studies (Catinella et al. 2005; Koopmann et al. 2006; Boselli & Gavazzi 2006) which have shown that the HI deficiency is associated with a truncation of the star forming disk. All the deficient objects lie at a projected distance of less than $\sim$1 degree from the center of Abell 1367, suggesting that the absence of HI and the truncation of the star formation disk is likely due to their interaction with the cluster environment. The fact that these objects have lost almost 40% of their original gas content but their broadband morphology and optical colours are still those typical of normal star forming spirals implies that they are recent arrivals within the cluster environment. It appears that the neutral hydrogen has been already stripped well within the optical radius quenching the star formation in the galaxy outskirts, but A type stars have not yet died and the galaxies still appear as blue as they were before losing their gas. Given that Hα traces stars younger than 2×10^7 yr and the typical lifetime of A stars is $\sim$1 Gyr, we can speculate that our galaxies started to loose their gas $\sim$100Myr ago, in agreement with the typical timescale for gas stripping observed in Virgo cluster galaxies (e.g. Vollmer et al. 2001, 2004; Boselli et al. 2006; Cortese et al. 2007) and predicted by numerical models (e.g. Abadi et al. 1999; Shioya et al. 2002; Roediger & Brüggen 2007). In less than 1 Gyr, when all the A stars are dead, these objects will lie in the $g-i$ red sequence and will not be any different from the bulk of the gas-poor (red) galaxy cluster population. Only future detailed spectroscopic investigation will allow us the better estimate the time scale of this transformation. Finally, it is interesting to note that this population of blue gas-poor galaxies corresponds to $\sim$ one third of the whole population of blue galaxies in the A1367-volume, supporting the idea that A1367 is a cluster still young and a considerable number of objects are infalling into the cluster core for the first time (Cortese et al. 2004).

[4] The Hα emission of a galaxy is due to the hydrogen ionized in HII regions by massive (>10 M$_\odot$), young ($< 2 \times 10^7$ yr) stars.

7 SUMMARY & CONCLUSIONS

We have presented the results of a HI blind survey of 5×1 square degrees centered on the core of Abell 1367 as part of the Arecibo Galaxy Environment Survey. One hundred HI galaxies have been detected (79 new measurements and 50 new redshifts), half of which belong to the Abell 1367 volume. Comparing the properties of the HI selected galaxies with an optically selected sample extracted from SDSS-DR5 we have shown that the large scale distribution of galaxies is strongly wavelength dependent: in HI the cluster core almost completely disappears and HI selected galaxies are homogeneously distributed in the cluster volume. The difference between the two samples is even more evident when we compare their luminosity and HI distribution. Our optically selected sample misses a considerable number of low luminosity, low surface brightness galaxies underestimating by almost a factor 2 the number of HI rich galaxies present in the cluster volume. On the contrary our HI sample contains a factor 3 less bright galaxies than the optical one. These are mainly ellipticals or early type, red spirals but also a not negligible fraction of the blue sequence cluster spirals is missed. All these blue gas-poor objects are located near the edge of the X-ray cluster contours suggesting that their gas has been recently ($\sim$ 100 Myr) stripped by ram pressure so that the galaxies are already gas poor whereas their stellar populations are still young.

Although the spatial and number distribution of samples selected at different wavelengths are significantly different, the internal properties of galaxies seem not to be significantly wavelengths dependent. HI galaxies seem to follow the same scaling relations observed in optical and bigger galaxies are redder, have a higher surface brightness and a lower gas content than lower luminosity galaxies. The most interesting result of our analysis is that the baryon fraction of our sample appears to be almost constant, suggesting the difference in the star to gas ratio observed between bright and faint galaxies is only due to a different star formation efficiency (i.e. the time scale necessary to convert gas into stars). This is the first time that such a result is obtained from an HI selected sample and even if consistent with models of galaxy formation it suggests that during their evolutionary history less massive galaxies do not lose a larger fraction of their baryons than bigger objects.

The analysis presented in this paper points out the importance of HI blind surveys like AGES in order to have an unbiased view of the properties of galaxies in the local Universe. Once the survey is at a more advanced stage and the size of our sample is significantly bigger than the one presented here it will be possible to carry out more detailed quantitative studies and comparisons between optically and HI selected samples, gaining more insight into the evolutionary history of nearby galaxies.

ACKNOWLEDGMENTS

LC wishes to thank all the AGES consortium and in particular Elias Brinks & Noah Brosh for useful discussions and comments on this manuscript. LC is supported by the UK Particle Physics and Astronomy Research Council.

This work is based on observations collected at Arecibo

Observatory. The Arecibo Observatory is part of the National Astronomy and Ionosphere Center, which is operated by Cornell University under a cooperative agreement with the National Science Foundation. We wish to thank the Arecibo Observatory for granting us the time to complete this part of the project and its staff for the help during the observations and data reduction. The TAC of the Loiano telescope is acknowledged for the time allocation to this project. This research has made use of the NASA/IPAC Extragalactic Database, which is operated by the Jet Propulsion Laboratory, California Institute of Technology, under contract to NASA and of the GOLDMine database (Gavazzi et al. 2003).

Funding for the SDSS and SDSS-II has been provided by the Alfred P. Sloan Foundation, the Participating Institutions, the National Science Foundation, the U.S. Department of Energy, the National Aeronautics and Space Administration, the Japanese Monbukagakusho, the Max Planck Society, and the Higher Education Funding Council for England. The SDSS Web Site is http://www.sdss.org/.

The SDSS is managed by the Astrophysical Research Consortium for the Participating Institutions. The Participating Institutions are the American Museum of Natural History, Astrophysical Institute Potsdam, University of Basel, University of Cambridge, Case Western Reserve University, University of Chicago, Drexel University, Fermilab, the Institute for Advanced Study, the Japan Participation Group, Johns Hopkins University, the Joint Institute for Nuclear Astrophysics, the Kavli Institute for Particle Astrophysics and Cosmology, the Korean Scientist Group, the Chinese Academy of Sciences (LAMOST), Los Alamos National Laboratory, the Max-Planck-Institute for Astronomy (MPIA), the Max-Planck-Institute for Astrophysics (MPA), New Mexico State University, Ohio State University, University of Pittsburgh, University of Portsmouth, Princeton University, the United States Naval Observatory, and the University of Washington.

REFERENCES

Abadi, M. G., Moore, B., & Bower, R. G. 1999, MNRAS, 308, 947
Adelman-McCarthy, J. K., Agüeros, M. A., Allam, S. S., et al. 2007, ApJS, 172, 634
Auld, R., Minchin, R. F., Davies, J. I., et al. 2006, MNRAS, 371, 1617
Baldry, I. K., Glazebrook, K., Brinkmann, J., et al. 2004, ApJ, 600, 681
Barnes, D. G., Staveley-Smith, L., de Blok, W. J. G., et al. 2001, MNRAS, 322, 486
Basilakos, S., Plionis, M., Kovač, K., & Voglis, N. 2007, MNRAS, 370
Bell, E. F., McIntosh, D. H., Katz, N., & Weinberg, M. D. 2003a, ApJL, 585, L117
Bell, E. F., McIntosh, D. H., Katz, N., & Weinberg, M. D. 2003b, ApJS, 149, 289
Boselli, A., Boissier, S., Cortese, L., et al. 2006, ApJ, 651, 811
Boselli, A. & Gavazzi, G. 2006, PASP, 118, 517
Boselli, A., Lequeux, J., & Gavazzi, G. 2002, A&A, 384, 33
Briggs, F. H. & Rao, S. 1993, ApJ, 417, 494
Buat, V., Takeuchi, T. T., Iglesias-Paramo, J., et al. 2007, ApJS in press (astro-ph/0609738)
Bullock, J. S., Dekel, A., Kolatt, T. S., et al. 2001, ApJ, 555, 240
Catinella, B., Haynes, M. P., & Giovanelli, R. 2005, AJ, 130, 1037
Cayatte, V., Kotanyi, C., Balkowski, C., & van Gorkom, J. H. 1994, AJ, 107, 1003
Chincarini, G. L., Giovanelli, R., & Haynes, M. P. 1983, ApJ, 269, 13
Cole, S., Lacey, C. G., Baugh, C. M., & Frenk, C. S. 2000, MNRAS, 319, 168
Cortese, L., Boselli, A., Gavazzi, G., et al. 2005, ApJL, 623, L17
Cortese, L., Gavazzi, G., Boselli, A., et al. 2006, A&A, 453, 847
Cortese, L., Gavazzi, G., Boselli, A., Iglesias-Paramo, J., & Carrasco, L. 2004, A&A, 425, 429
Cortese, L., Gavazzi, G., Iglesias-Paramo, J., Boselli, A., & Carrasco, L. 2003, A&A, 401, 471
Cortese, L., Marcillac, D., Richard, J., et al. 2007, MNRAS, 376, 157
Cowie, L. L., Songaila, A., Hu, E. M., & Cohen, J. G. 1996, AJ, 112, 839
Crain, R. A., Eke, V. R., Frenk, C. S., et al. 2007, MNRAS, 377, 41
Davies, J., Minchin, R., Sabatini, S., et al. 2004, MNRAS, 349, 922
Davies, J. I., de Blok, W. J. G., Smith, R. M., et al. 2001, MNRAS, 328, 1151
De Propris, R., Colless, M., Driver, S. P., et al. 2003, MNRAS, 342, 725
Dressler, A. 1980, ApJ, 236, 351
Freeman, K. C. 1970, ApJ, 160, 811
Freudling, W., Staveley-Smith, L., Calabretta, M., et al. 2005, in Bulletin of the American Astronomical Society, Vol. 37, Bulletin of the American Astronomical Society, 1316–+
Gavazzi, G. 1987, ApJ, 320, 96
Gavazzi, G. 1989, ApJ, 346, 59
Gavazzi, G., Boselli, A., Donati, A., Franzetti, P., & Scodeggio, M. 2003, A&A, 400, 451
Gavazzi, G., Boselli, A., van Driel, W., & O'Neil, K. 2005, A&A, 429, 439
Gavazzi, G., Franzetti, P., Scodeggio, M., Boselli, A., & Pierini, D. 2000, A&A, 361, 863
Gavazzi, G., O'Neil, K., Boselli, A., & van Driel, W. 2006, A&A, 449, 929
Gavazzi, G., Pierini, D., & Boselli, A. 1996, A&A, 312, 397
Geha, M., Blanton, M. R., Masjedi, M., & West, A. A. 2006, ApJ, 653, 240
Giovanelli, R. & Haynes, M. P. 1985, ApJ, 292, 404
Giovanelli, R., Haynes, M. P., Herter, T., et al. 1997, AJ, 113, 22
Giovanelli, R., Haynes, M. P., Kent, B. R., et al. 2005, AJ, 130, 2598
Giovanelli, R., Haynes, M. P., Kent, B. R., et al. 2007, AJ, 133, 2569
Girardi, M., Giuricin, G., Mardirossian, F., Mezzetti, M., & Boschin, W. 1998, ApJ, 505, 74
Governato, F., Willman, B., Mayer, L., et al. 2007, MNRAS, 374, 1479

Haynes, M. P. & Giovanelli, R. 1984, AJ, 89, 758
Haynes, M. P., Giovanelli, R., Herter, T., et al. 1997, AJ, 113, 1197
Henning, P. A., Springob, C. M., Catinella, B., et al. 2006, in American Astronomical Society Meeting Abstracts, Vol. 208, American Astronomical Society Meeting Abstracts, 53.04–+
Henning, P. A., Staveley-Smith, L., Ekers, R. D., et al. 2000, AJ, 119, 2686
Higdon, S. J. U., Armus, L., Higdon, J. L., Soifer, B. T., & Spoon, H. W. W. 2006, ApJ, 648, 323
Iglesias-Páramo, J., Boselli, A., Cortese, L., Vílchez, J. M., & Gavazzi, G. 2002, A&A, 384, 383
Kauffmann, G., Heckman, T. M., White, S. D. M., et al. 2003, MNRAS, 341, 33
Kennicutt, Jr., R. C., Bothun, G. D., & Schommer, R. A. 1984, AJ, 89, 1279
Koopmann, R. A., Haynes, M. P., & Catinella, B. 2006, AJ, 131, 716
Koribalski, B. S., Staveley-Smith, L., Kilborn, V. A., et al. 2004, AJ, 128, 16
Lang, R. H., Boyce, P. J., Kilborn, V. A., et al. 2003, MNRAS, 342, 738
Lewis, B. M. 1983, AJ, 88, 962
McGaugh, S. & de Blok, E. 1998, in Astronomical Society of the Pacific Conference Series, Vol. 136, Galactic Halos, ed. D. Zaritsky, 210–+
McGaugh, S. S., Schombert, J. M., Bothun, G. D., & de Blok, W. J. G. 2000, ApJL, 533, L99
Meyer, M. J., Zwaan, M. A., Webster, R. L., Brown, M. J. I., & Staveley-Smith, L. 2007, ApJ, 654, 702
Minchin, R. F., Auld, R., Davies, J. I., et al. 2007, in IAU Symposium, Vol. 235, IAU Symposium, ed. F. Combes & J. Palous, 227–229
Minchin, R. F., Disney, M. J., Boyce, P. J., et al. 2003, MNRAS, 346, 787
Minchin, R. F., Momjian, E., Cortese, L., et al. 2006, in American Astronomical Society Meeting Abstracts, 95.03–+
Roediger, E. & Brüggen, M. 2007, MNRAS, 765
Rosenberg, J. L. & Schneider, S. E. 2000, ApJS, 130, 177
Saintonge, A. 2007, AJ, 133, 2087
Sakai, S., Mould, J. R., Hughes, S. M. G., et al. 2000, ApJ, 529, 698
Salpeter, E. E. & Hoffman, G. L. 1996, ApJ, 465, 595
Sault, R. J., Teuben, P. J., & Wright, M. C. H. 1995, in ASP Conf. Ser. 77: Astronomical Data Analysis Software and Systems IV, ed. R. A. Shaw, H. E. Payne, & J. J. E. Hayes, 433–+
Shioya, Y., Bekki, K., Couch, W. J., & De Propris, R. 2002, ApJ, 565, 223
Solanes, J. M., Giovanelli, R., & Haynes, M. P. 1996, ApJ, 461, 609
Solanes, J. M., Manrique, A., García-Gómez, C., et al. 2001, ApJ, 548, 97
Spitzak, J. G. & Schneider, S. E. 1998, ApJS, 119, 159
Springob, C. M., Haynes, M. P., & Giovanelli, R. 2005a, ApJ, 621, 215
Springob, C. M., Haynes, M. P., Giovanelli, R., & Kent, B. R. 2005b, ApJS, 160, 149
Sullivan, III, W. T., Bates, B., Bothun, G. D., & Schommer, R. A. 1981, AJ, 86, 919
Swaters, R. A., van Albada, T. S., van der Hulst, J. M., & Sancisi, R. 2002, A&A, 390, 829
Tschöke, D., Bomans, D. J., Hensler, G., & Junkes, N. 2001, A&A, 380, 40
Vollmer, B., Balkowski, C., Cayatte, V., van Driel, W., & Huchtmeier, W. 2004, A&A, 419, 35
Vollmer, B., Cayatte, V., Balkowski, C., & Duschl, W. J. 2001, ApJ, 561, 708
Whitmore, B. C., Gilmore, D. M., & Jones, C. 1993, ApJ, 407, 489
Wong, O. I., Ryan-Weber, E. V., Garcia-Appadoo, D. A., et al. 2006, MNRAS, 371, 1855
Zabludoff, A. I., Geller, M. J., Huchra, J. P., & Ramella, M. 1993, AJ, 106, 1301

APPENDIX: INTERESTING OBJECTS

High Velocity Clouds Two extended features well separated from the Milky Way emission and probably associated with High Velocity Clouds (HVCs) have been detected in the velocity range 140< V <210 km s^{-1}(Fig.13). The first lies in the range 11:50< $R.A.$ <11:55 and probably extends outside the region observed. The brightest region is in the south-east corner of the cube (11:54:00, +19:20:00, 160< V <210 km s^{-1}) and a low column density stream seems to extend to the north-west. The second and strongest HVC occupies great part of the east part of the cube and extends over 1.5 degrees (11:40< $R.A.$ <11:46, 19:25< $Dec.$ <20:15) with a velocity in the range 140< V <175 km s^{-1}.

CGCG97-027-group The CGCG97027-group is located at a projected distance of ∼2 degrees (∼3.2 Mpc) from the centre of Abell 1367. It is composed of two star forming spirals CGCG97027 (V∼6630 km s^{-1}) and CGCG97026 (V∼6220 km s^{-1}) and one lenticular CGCG97023 (V∼6320 km s^{-1}). At a projected distance of ∼13 arcmin (∼0.7 Mpc) SW from the group lies the elliptical galaxy CGCG97-021 (V∼6648 km s^{-1}). Our data show the presence of diffuse HI emission all over the region occupied by the four bright Zwicky galaxies (see Fig.14). In particular and high velocity 6500< V <6800 km s^{-1}streams extends from CGCG97-021 to the north (Fig.14, left) and two of the HI sources without optical counterparts belong to this stream (AGES J113614+195910 and AGES J113626+195102). Extended emission is also detected in the north part of the CGCG97-027 group in the velocity range 6000< V <6500 km s^{-1}(Fig.14, right).

CGCG97041-group : The CGCG97041-group is located at a projected distance of 1 degrees (1.6 Mpc) from the centre of Abell 1367 and, as the CGCG97027-group, it is composed of two spirals CGCG97036 (V∼6595 km s^{-1}) and AGC210559 (V∼6825 km s^{-1}) and one lenticular CGCG97041 (V∼6778 km s^{-1}). We detect HI emission extended over ∼200 kpc north of the three group members, apparently not associated with either of them (see Fig.15).

AGES J113939+193524 This source (V = 7382 km s^{-1}) has no optical counterpart catalogued in the SDSS database. However in the SDSS plates a low surface brightness ($\mu(i)$ ∼

24 mag arcsec^{-2} galaxy is present in correspondence of the HI coordinates. We considered this object as candidate optical counterpart and labeled it as SDSSLSB in Table 3.

AGES J114239+201150 This source lies at a projected distance of ∼5.8 arcmin from the starburst galaxy CGCG97-068. No galaxies or extended features are found in deep CFHT B-band (Gavazzi et al. 2003) and GALEX NUV-FUV (Cortese et al. 2005) data in correspondence with the peak of HI emission, suggesting that it could be a stream of gas stripped from CGCG97-068. Unfortunately the distance of the source from CGCG97-068 is consistent with the region in which the first sidelobe is expected and the fact that AGES J114239+201150 lies at exactly the same recessional velocity of the starburst galaxy makes impossible to discard the possibility that this source is sidelobe contaminated.

VLA D-configuration observations has been recently obtained for the interacting groups described above and for CGCG97-068 and will be used to study in detail the properties of these sources. The results of these observations will be presented in a forthcoming work.

AGES J114809+192109 This source (V = 11252 km s^{-1}) lies at the south edge of our cube and it is not clearly associated with any optical galaxy.

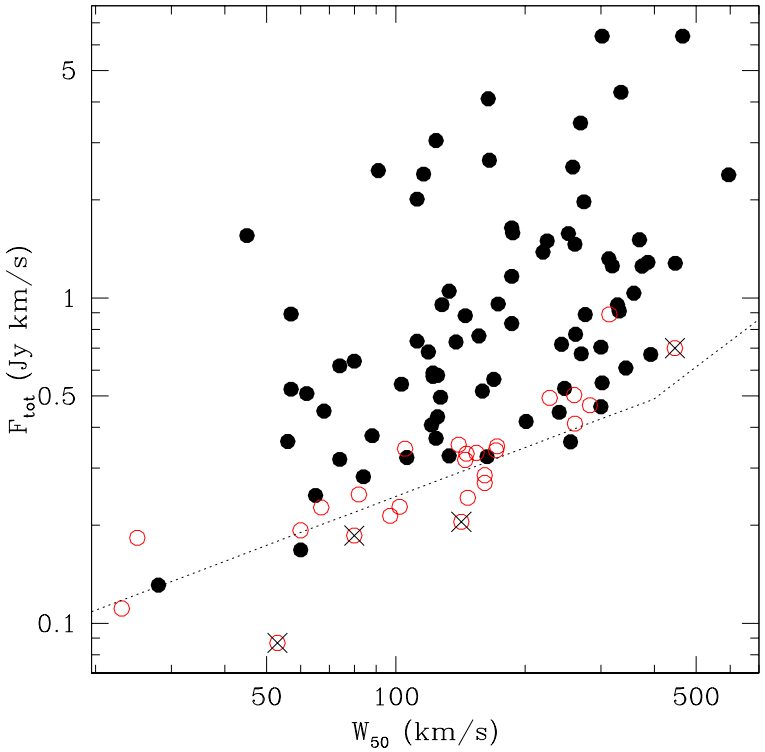

Figure 1. The distribution of the 104 HI source candidates detected in the AGES-A1367 cube. Filled circles indicate "sure" sources (i.e. detected by all the three extraction methods adopted), empty circles are sources not detected by all the three extraction methods and investigated with follow-up Lwide observations (see Sec.3). Crosses indicate those sources that have not been confirmed by follow-up observations. The dotted line shows the ALFALFA reliability limit, $S/N_{tot} = 6.5$ (Saintonge 2007).

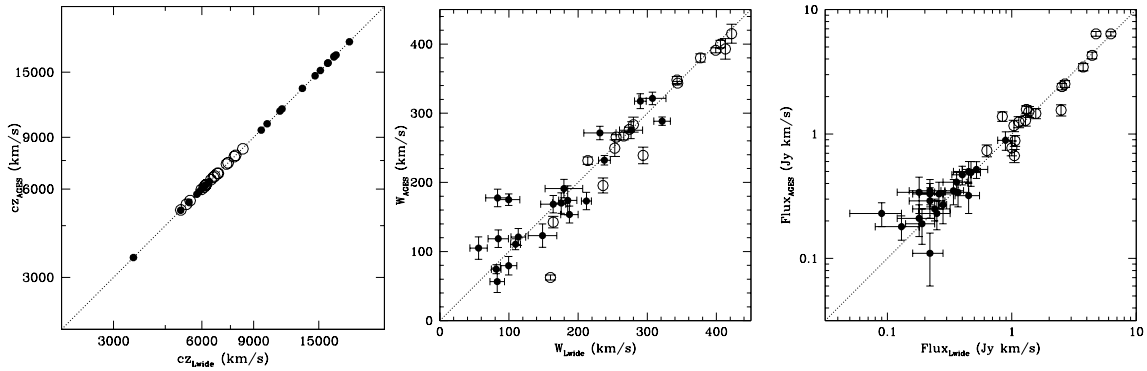

Figure 2. Comparison of the recessional velocities (Left), the velocity widths (Center) and the HI fluxes measured by AGES and L-wide. Filled circles indicate the 22 sources confirmed during follow-up observations, empty circles show the 18 galaxies already known from the literature . The dotted lines indicate a one to one correlation.

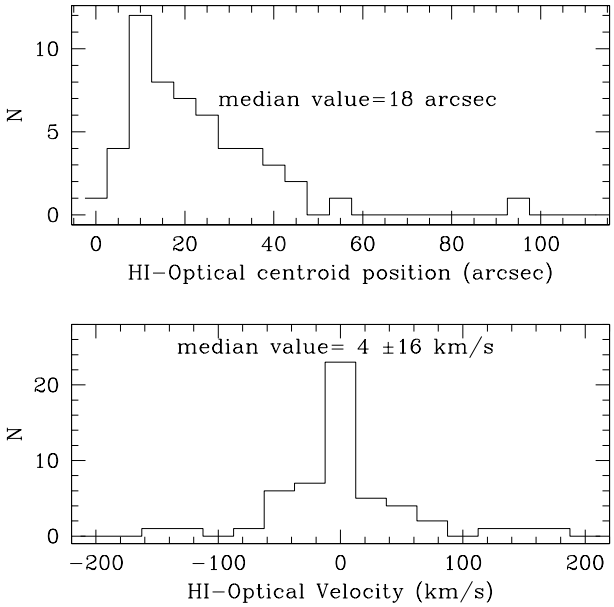

Figure 3. Distribution of the positional (upper panel) and recessional velocity (lower panel) difference between the HI sources and their optical counterparts.

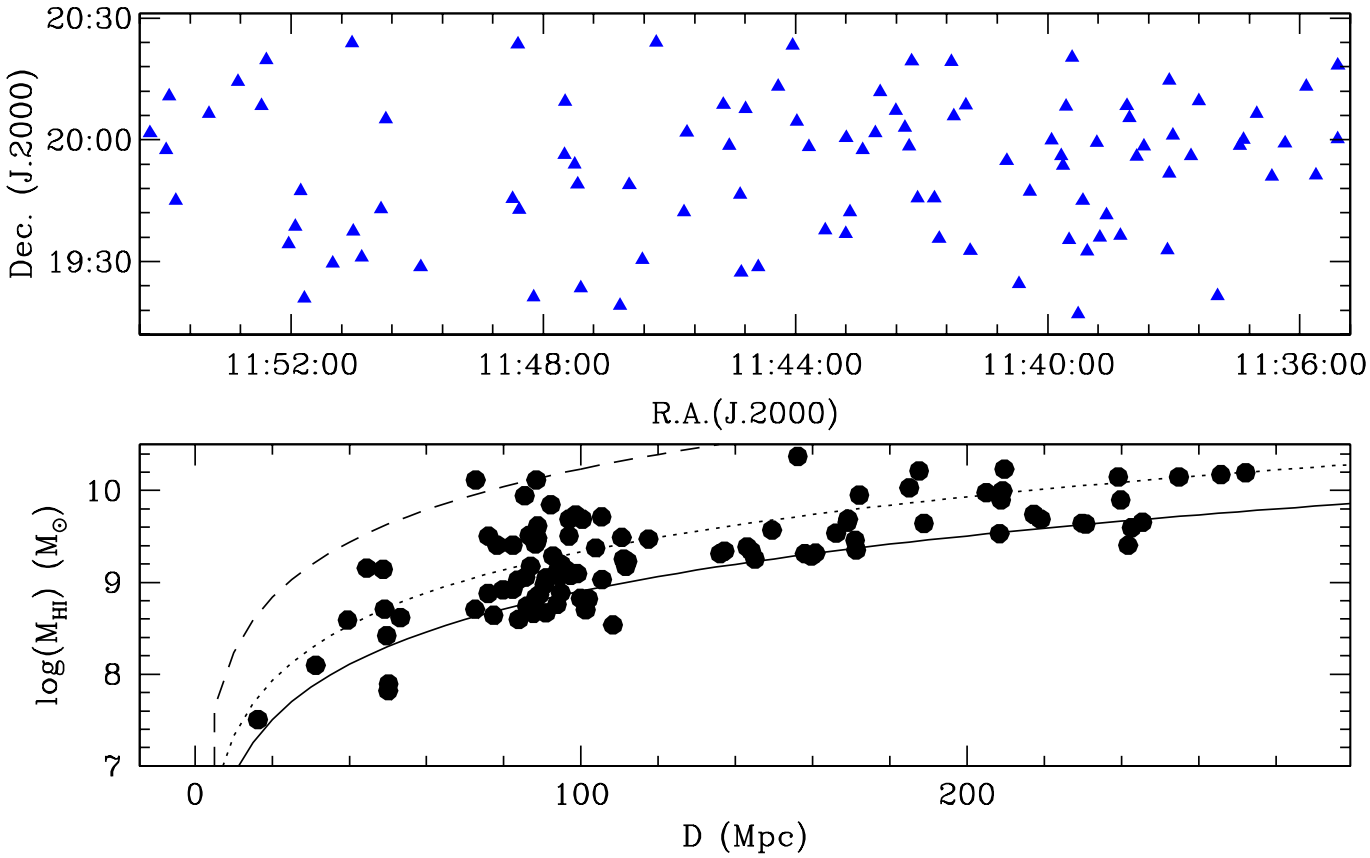

Figure 4. The sky (upper panel) and HI mass vs distance (lower panel) distribution for the 100 HI sources in our sample. In the lower panel distances are obtained from the recessional velocities assuming that all galaxies are in the Hubble flow. The solid line shows the sensitivity limit for a $S/N_{tot} \sim 6.5$ source having W_{50} of 200 km s^{-1}. The dotted line show the ALFALFA reliability limit for the same velocity width (Giovanelli et al. 2007). The dashed line indicates a flux integral of 7.3 Jy km s^{-1}, which corresponds to the HIPASS 6.5σ limit for a velocity width of 200 km s^{-1}.

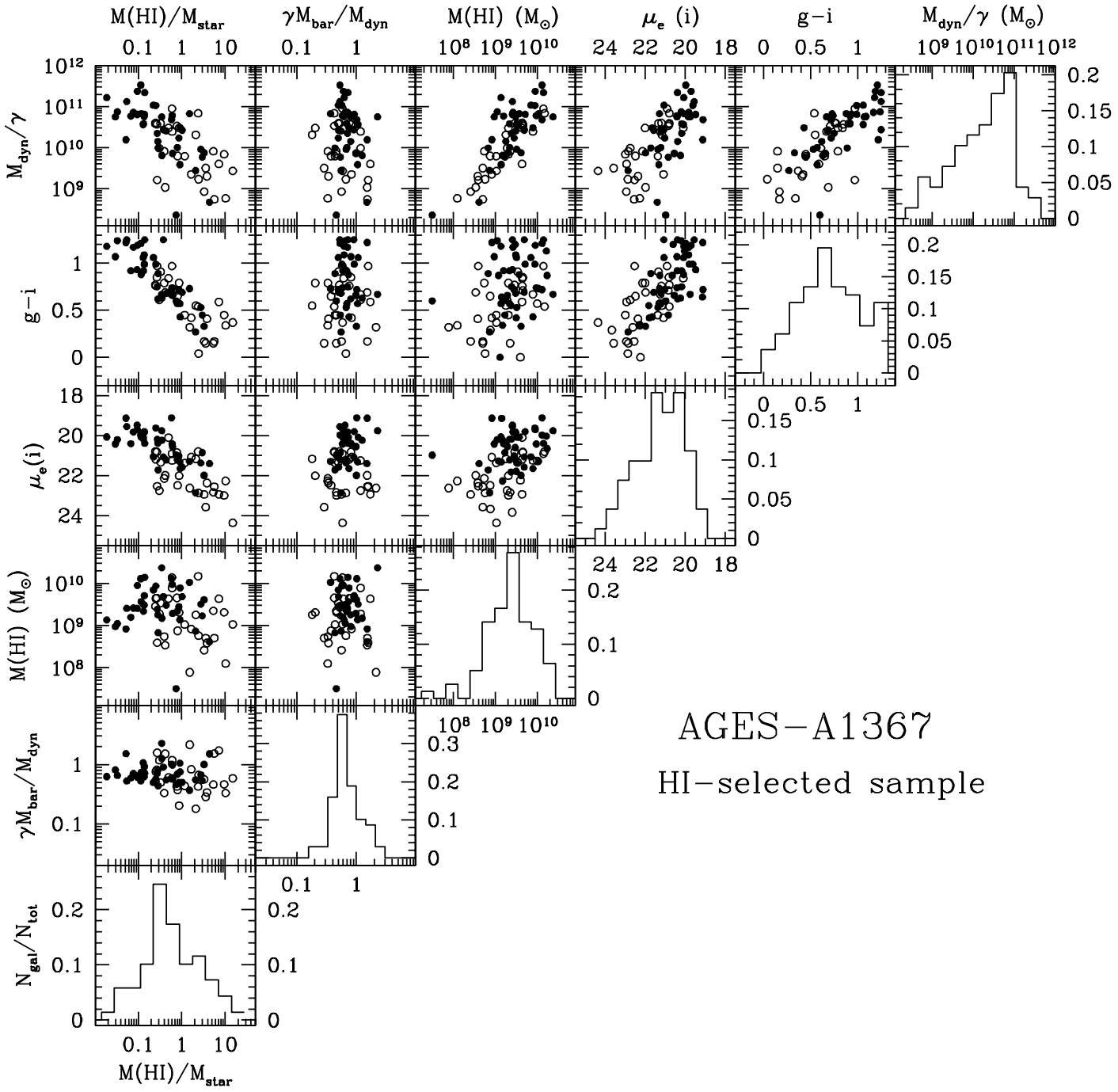

Figure 5. Distributions and correlations between HI and optical properties for the 69 galaxies in our sample having 1 optical counterpart and $e > 0.1$. From left to right the ratio of the gas to stellar mass, the baryons fraction, the total HI mass, the effective surface brightness in i band, the $g-i$ color and the dynamical mass are presented. Filled dots are objects with confirmed optical counterparts while empty dots indicates objects with optical counterpart candidates.

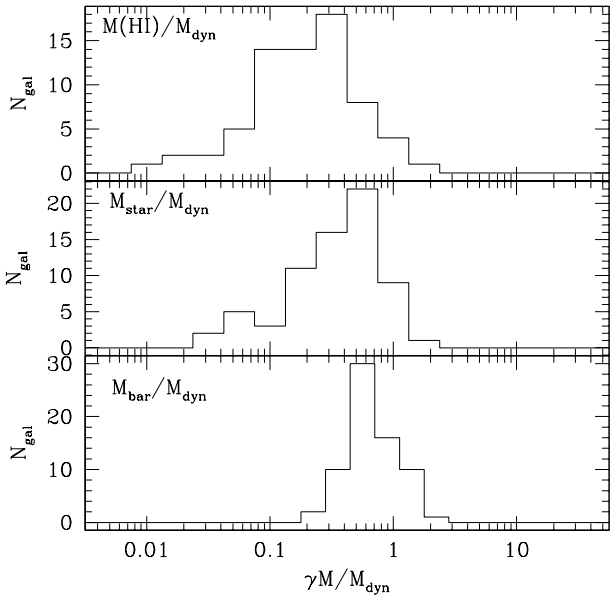

Figure 6. The distribution of the gas to dynamical mass (top), star to dynamical mass (middle) and baryon to dynamical mass (bottom) ratios for our sample.

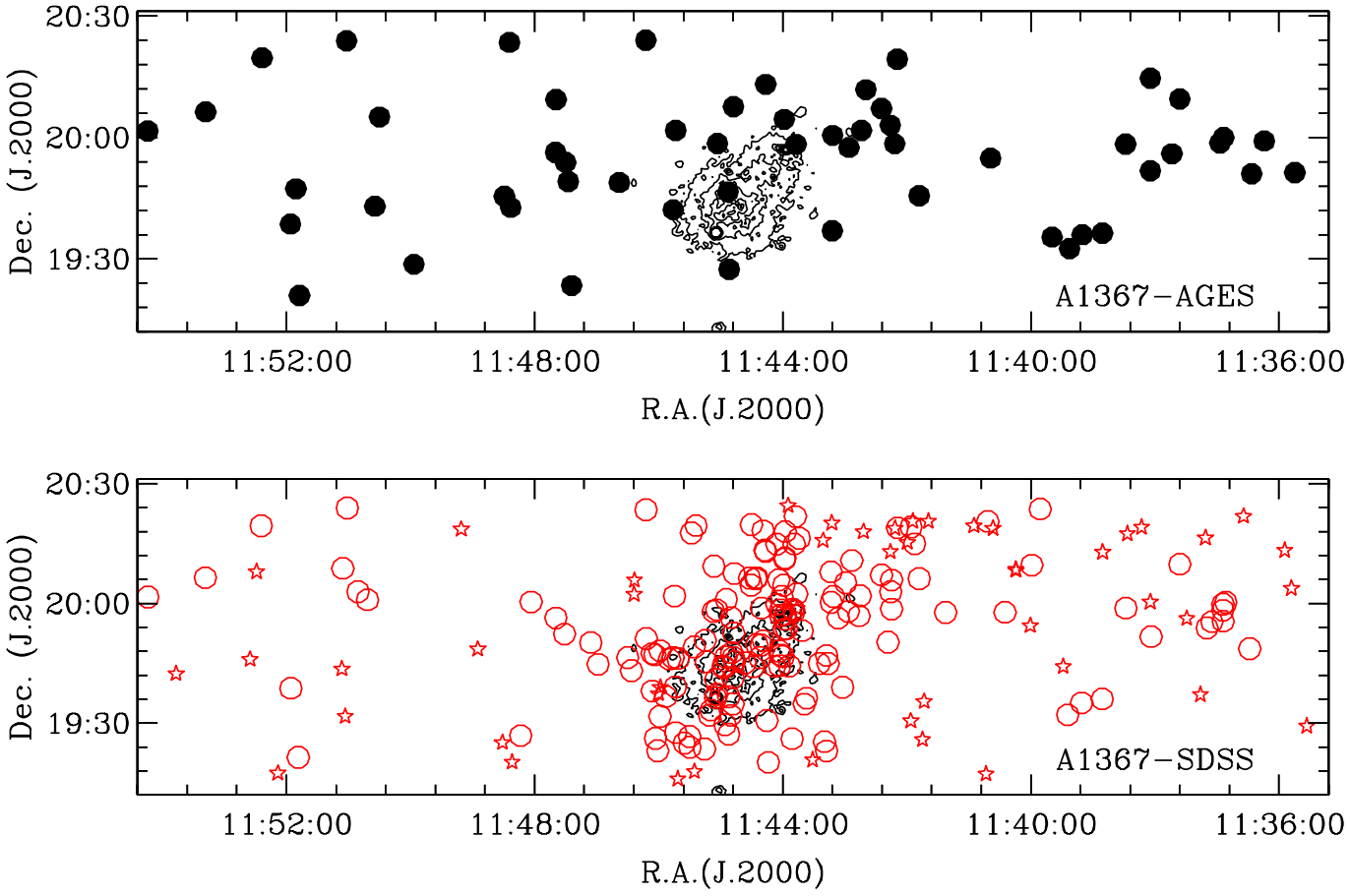

Figure 7. Upper panel: Sky distribution of the members ($4000< V <10000$ km s^{-1}) of the Abell 1367 cluster in the HI selected sample. Lower panel: Sky distribution of galaxies in the SDSS optically selected sample (g <17 mag). Empty circles indicate confirmed cluster members and empty stars galaxies without redshift available. The black contours indicate the X-ray emission from A1367 as measured by ROSAT.

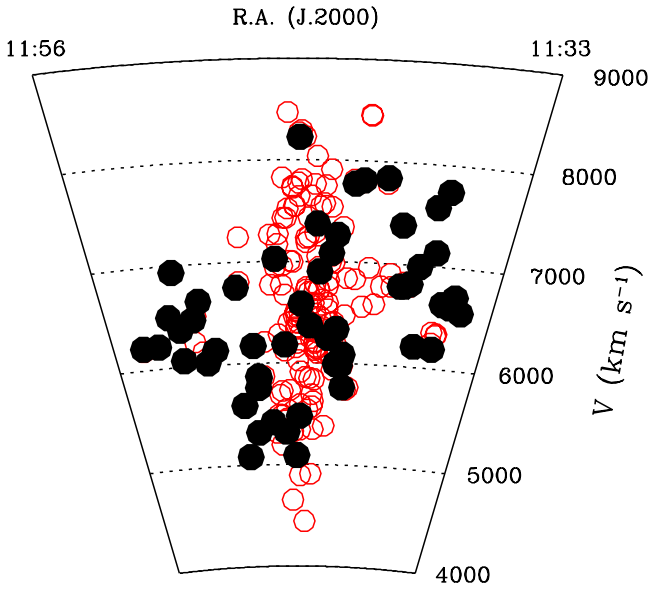

Figure 8. The wedge diagram of the AGES-A1367 region in the velocity range $4000< V <9000$ km s^{-1}. Filled circles indicate the HI detections while empty circles are galaxies belonging to the SDSS optical selected sample (g <17 mag).

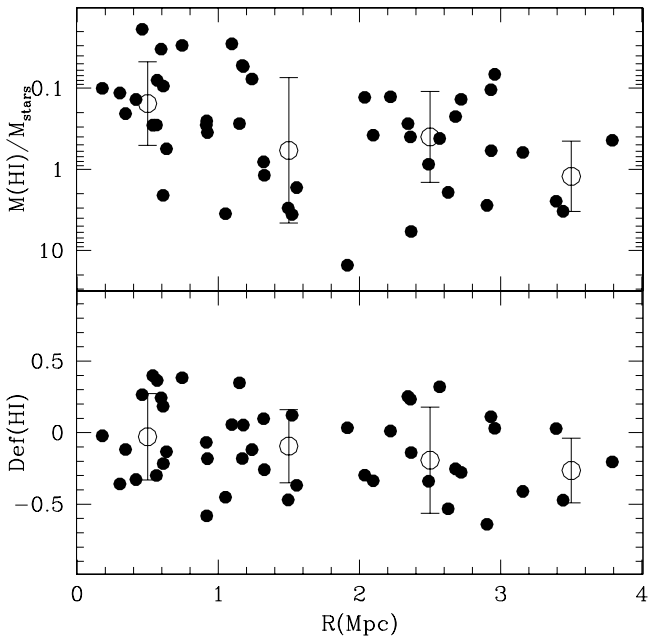

Figure 9. The distribution of the gas to star mass ratio (upper panel) and of the HI deficiency as a function of the projected distance from the center of Abell 1367. Empty circles show the average values and standard deviations obtained in bins 1 Mpc wide.

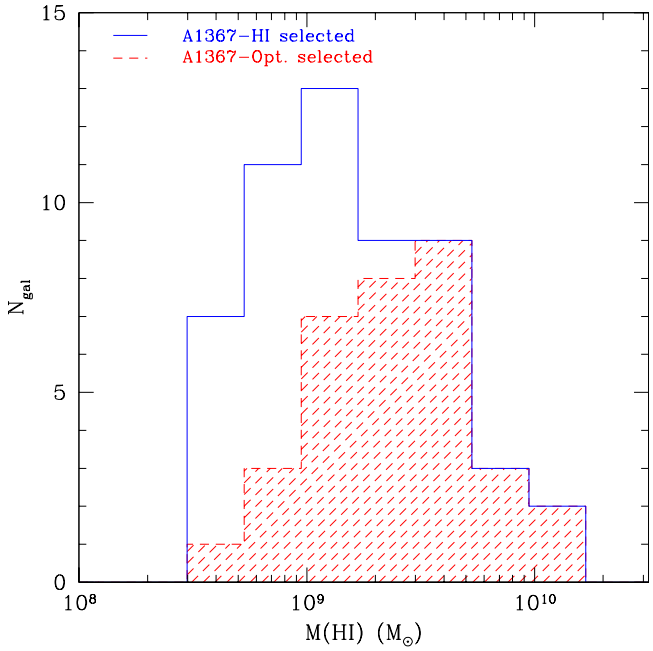

Figure 10. The HI mass distribution for galaxies in the A1367 volume. The solid histogram indicates the HI selected sample and the shaded histogram the optically selected sample extracted from SDSS-DR5 ($g < 17$ mag).

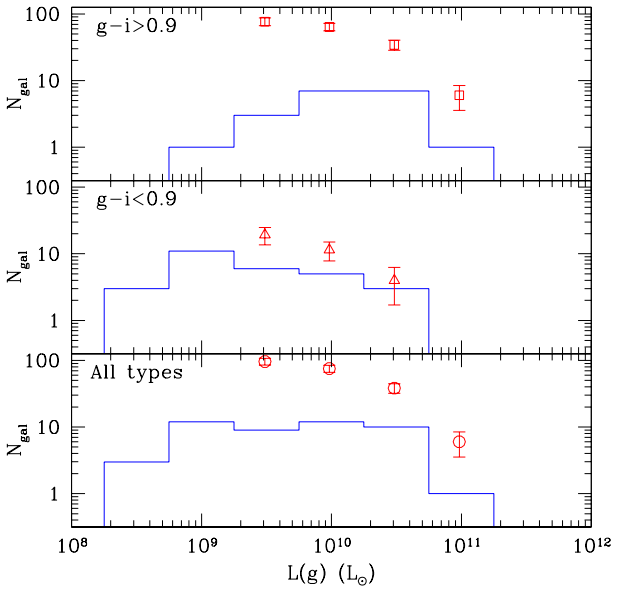

Figure 11. Each panel shows the g band luminosity function for galaxies in the A1367 volume as obtained from the optically (empty circles) and HI (histogram) selected sample. All galaxies in the two samples are shown in the bottom panel, while blue ($g - i$ <0.9) and red galaxies ($g - i$ >0.9) are shown in the middle and upper panel respectively.

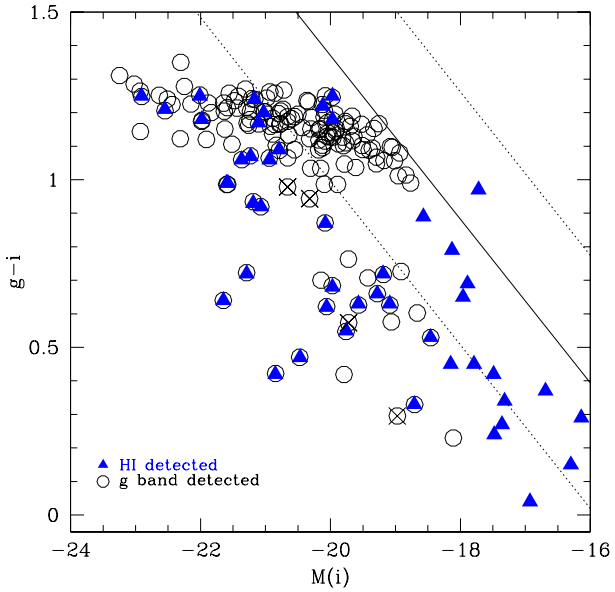

Figure 12. The $g-i$ color $M(i)$ magnitude relation for confirmed cluster members in the Abell 1367 region. Triangles indicate galaxies detected in the AGES cube. Crosses indicate those galaxies lying in the RFIs velocity range or within the beam occupied by brighter sources. The solid (dashed) line indicate our sensitivity limit (±1 σ) obtained converting the HI sensitivity into color limit using the $g-i$ versus $M(HI)/L(i)$ relation given by Eq.6.

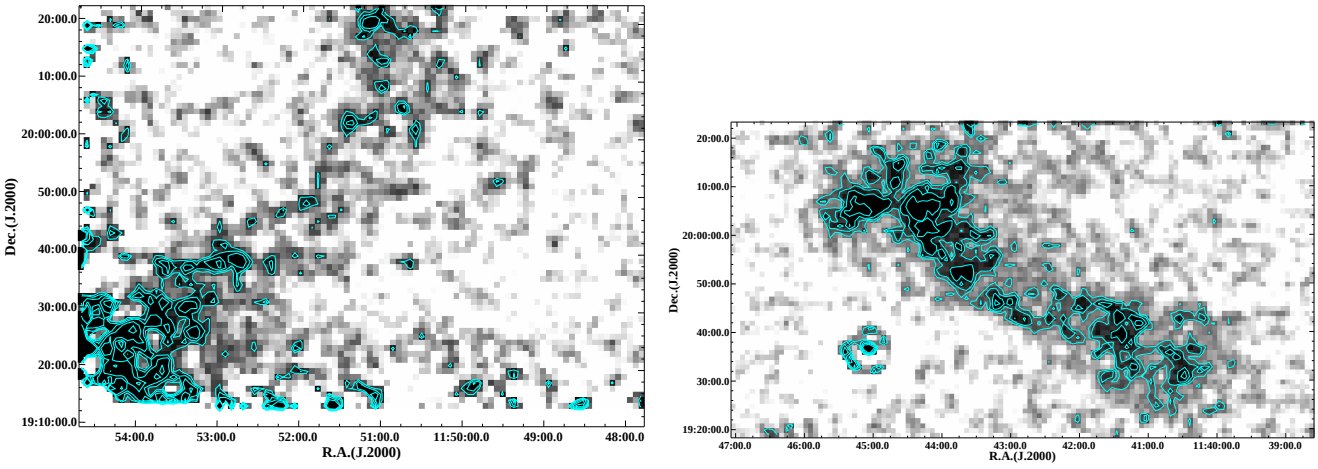

Figure 13. The two High velocity clouds complexes detected in the AGES-A1367 cube. The HI column density maps were obtained integrating the line emission in the data cube within the velocity range 160< V <210 km s^{-1}(left) and 140< V <175 km s^{-1}(right). Contours are superposed to the moment map: 0.08, 0.1, 0.12, 0.16 Jy km s^{-1}beam^{-1}.

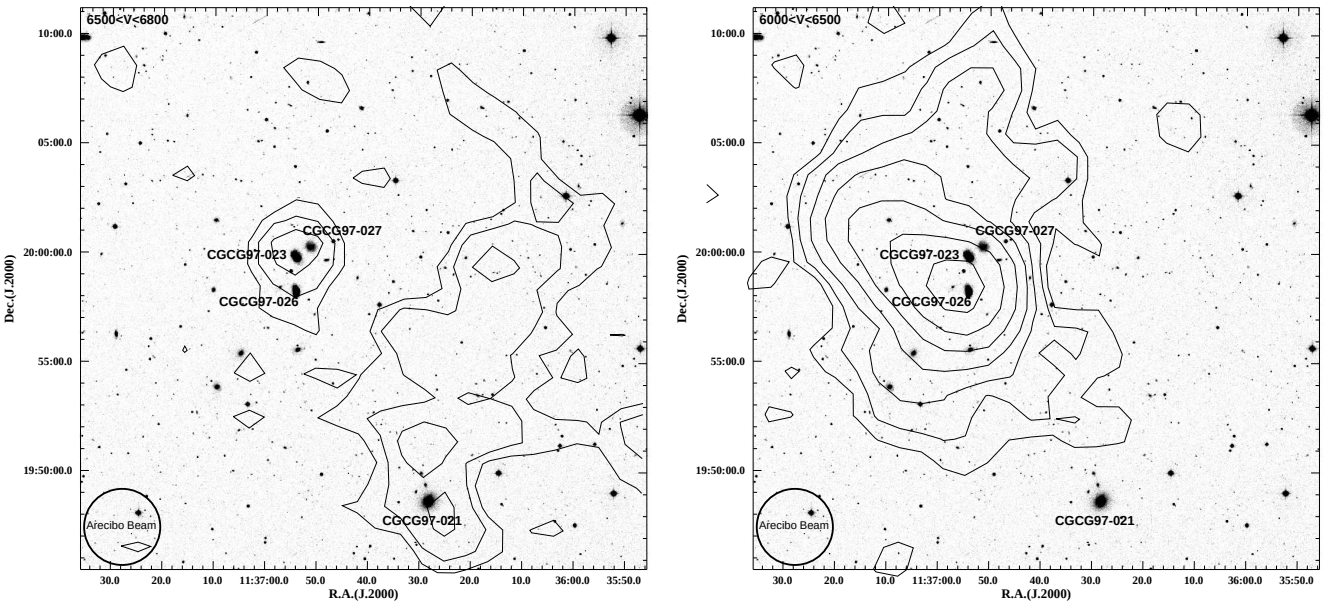

Figure 14. The CGCG97-027 group as seen on the DSS-blue plates. HI columns density contours were obtained from moment maps of the AGES data cube in the velocity range 6500< V <6850 km s^{-1}(left) and 6000< V <6500 km s^{-1}are superposed. Contours levels are: 0.2, 0.3, 0.5 Jy km s^{-1}beam^{-1} (left) and 0.3, 0.46, 0.71, 1.1, 1.7, 2.6, 4 Jy km s^{-1}beam^{-1} (right).

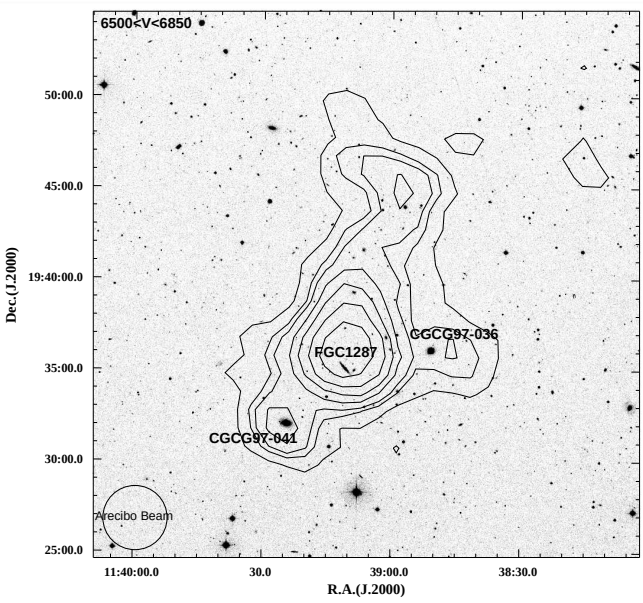

Figure 15. The CGCG97-041 group as seen on the DSS-blue plates. Radio contours obtained from moment maps of the AGES cube in the velocity range 6500< V <6850 km s^{-1}. Contours levels are: 0.18, 0.26, 0.36, 0.52, 0.73, 1.05, 1.5 Jy km s^{-1}beam^{-1}.

Table 1. HI parameters for the 100 sources detected in the Abell 1367 cube.

$HI-ID$	$R.A.$ (J.2000)	$\sigma_{R.A.}$ sec.	$Dec.$ (J.2000)	$\sigma_{Dec.}$ arcsec	V km s^{-1}	$W50$ km s^{-1}	$W20$ km s^{-1}	F_{peak} mJy	F_{tot} Jy km s^{-1}	$flag$
$AGES$ $J113444+201217$	11 : 34 : 44.4	0.7	20 : 12 : 17	11	9602 ± 6	127 ± 12	181 ± 18	5.5 ± 0.7	0.50 ± 0.08	0
$AGES$ $J113508+201210$	11 : 35 : 08.8	0.7	20 : 12 : 10	10	16152 ± 7	105 ± 14	137 ± 20	3.5 ± 0.6	0.35 ± 0.08	1
$AGES$ $J113523+201823$	11 : 35 : 23.8	0.7	20 : 18 : 23	10	10464 ± 6	300 ± 11	344 ± 17	5.0 ± 0.7	0.71 ± 0.10	0
$AGES$ $J113524+200009$	11 : 35 : 24.2	0.8	20 : 00 : 09	13	9523 ± 3	283 ± 7	294 ± 10	3.4 ± 0.5	0.47 ± 0.08	1
$AGES$ $J113544+195120$	11 : 35 : 44.8	0.8	19 : 51 : 20	11	6564 ± 7	84 ± 14	120 ± 20	3.7 ± 0.6	0.28 ± 0.07	0
$AGES$ $J113553+201308$	11 : 35 : 53.9	0.7	20 : 13 : 08	11	1142 ± 4	62 ± 7	103 ± 11	8.8 ± 0.7	0.51 ± 0.07	0
$AGES$ $J113614+195910$	11 : 36 : 14.3	0.8	19 : 59 : 10	13	6713 ± 11	119 ± 22	273 ± 33	4.9 ± 0.6	0.68 ± 0.10	0
$AGES$ $J113626+195102$	11 : 36 : 26.5	0.8	19 : 51 : 02	12	6609 ± 9	122 ± 19	204 ± 28	4.8 ± 0.7	0.57 ± 0.10	0
$AGES$ $J113641+200622$	11 : 36 : 41.2	0.7	20 : 06 : 22	10	18604 ± 8	276 ± 17	336 ± 25	4.6 ± 0.7	0.89 ± 0.13	0
$AGES$ $J113653+200003$	11 : 36 : 53.7	0.7	20 : 00 : 03	11	6637 ± 6	262 ± 12	305 ± 18	4.7 ± 0.6	0.77 ± 0.11	0
$AGES$ $J113657+195837$	11 : 36 : 57.1	0.7	19 : 58 : 37	10	6190 ± 3	302 ± 7	394 ± 10	26.6 ± 1.4	6.38 ± 0.28	0
$AGES$ $J113718+192129$	11 : 37 : 18.4	0.7	19 : 21 : 29	10	14348 ± 5	328 ± 11	355 ± 16	4.9 ± 0.7	0.95 ± 0.13	0
$AGES$ $J113736+200934$	11 : 37 : 36.0	0.7	20 : 09 : 34	11	7739 ± 3	369 ± 7	391 ± 10	8.7 ± 0.9	1.51 ± 0.15	0
$AGES$ $J113743+195559$	11 : 37 : 43.7	0.8	19 : 55 : 59	13	7135 ± 8	106 ± 15	144 ± 23	3.4 ± 0.6	0.32 ± 0.08	2
$AGES$ $J113801+200106$	11 : 38 : 01.0	0.8	20 : 01 : 06	12	19052 ± 5	314 ± 10	329 ± 15	4.5 ± 0.8	0.90 ± 0.15	1
$AGES$ $J113804+195146$	11 : 38 : 04.5	0.7	19 : 51 : 46	10	6203 ± 3	220 ± 6	243 ± 9	8.1 ± 0.7	1.39 ± 0.12	0
$AGES$ $J113804+201441$	11 : 38 : 04.5	1.0	20 : 14 : 41	11	7580 ± 4	60 ± 7	80 ± 11	3.7 ± 0.4	0.17 ± 0.04	0
$AGES$ $J113805+193250$	11 : 38 : 05.9	0.7	19 : 32 : 50	10	17843 ± 3	331 ± 7	352 ± 10	6.0 ± 0.7	0.91 ± 0.11	0
$AGES$ $J113828+195823$	11 : 38 : 28.5	0.7	19 : 58 : 23	11	6989 ± 2	133 ± 4	144 ± 6	7.9 ± 0.7	0.33 ± 0.06	2
$AGES$ $J113835+195550$	11 : 38 : 35.5	1.0	19 : 55 : 50	17	13218 ± 6	301 ± 12	334 ± 18	2.7 ± 0.4	0.52 ± 0.07	1
$AGES$ $J113842+200527$	11 : 38 : 42.4	0.8	20 : 05 : 27	11	3513 ± 4	28 ± 7	49 ± 11	4.7 ± 0.6	0.13 ± 0.04	0
$AGES$ $J113844+200821$	11 : 38 : 44.8	0.7	20 : 08 : 21	10	3113 ± 1	124 ± 3	138 ± 4	25.7 ± 1.4	3.04 ± 0.19	0
$AGES$ $J113850+193622$	11 : 38 : 50.8	1.8	19 : 36 : 22	21	6811 ± 6	122 ± 11	196 ± 17	6.1 ± 0.6	0.59 ± 0.07	0
$AGES$ $J113904+194129$	11 : 39 : 04.2	0.7	19 : 41 : 29	11	16984 ± 7	161 ± 14	194 ± 21	4.0 ± 0.7	0.29 ± 0.08	1
$AGES$ $J113910+193558$	11 : 39 : 10.3	0.7	19 : 35 : 58	10	6783 ± 7	116 ± 13	383 ± 20	15.4 ± 0.9	2.40 ± 0.15	0
$AGES$ $J113913+195915$	11 : 39 : 13.2	1.0	19 : 59 : 15	12	10153 ± 6	255 ± 12	292 ± 18	3.5 ± 0.5	0.36 ± 0.07	0
$AGES$ $J113922+193232$	11 : 39 : 22.6	0.8	19 : 32 : 32	13	6783 ± 3	252 ± 5	282 ± 8	9.8 ± 0.7	1.58 ± 0.11	0
$AGES$ $J113926+194459$	11 : 39 : 26.7	0.7	19 : 44 : 59	15	17182 ± 12	145 ± 23	203 ± 35	2.7 ± 0.6	0.32 ± 0.09	1
$AGES$ $J113930+191706$	11 : 39 : 30.9	0.7	19 : 17 : 06	10	3438 ± 3	57 ± 6	85 ± 9	15.3 ± 1.3	0.89 ± 0.12	0
$AGES$ $J113936+202020$	11 : 39 : 36.9	0.7	20 : 20 : 20	12	16743 ± 4	358 ± 7	370 ± 11	5.2 ± 0.8	1.03 ± 0.15	0
$AGES$ $J113939+193524$	11 : 39 : 39.5	0.7	19 : 35 : 24	10	7382 ± 4	57 ± 8	104 ± 12	8.5 ± 0.7	0.52 ± 0.07	0
$AGES$ $J113942+200817$	11 : 39 : 42.4	0.8	20 : 08 : 17	12	16920 ± 9	25 ± 18	185 ± 27	5.3 ± 0.6	0.18 ± 0.04	1
$AGES$ $J113945+195341$	11 : 39 : 45.2	0.7	19 : 53 : 41	10	11177 ± 4	74 ± 7	103 ± 11	4.6 ± 0.5	0.32 ± 0.05	0
$AGES$ $J113947+195559$	11 : 39 : 47.3	0.7	19 : 55 : 59	10	10933 ± 3	164 ± 6	246 ± 10	24.8 ± 1.3	4.09 ± 0.21	0
$AGES$ $J113956+195955$	11 : 39 : 56.1	0.7	19 : 59 : 55	11	10090 ± 4	240 ± 7	248 ± 11	3.1 ± 0.6	0.45 ± 0.09	0
$AGES$ $J114016+194715$	11 : 40 : 16.9	0.7	19 : 47 : 15	11	3476 ± 3	68 ± 6	96 ± 9	6.9 ± 0.6	0.45 ± 0.06	0
$AGES$ $J114027+192429$	11 : 40 : 27.5	0.7	19 : 24 : 29	10	3411 ± 3	91 ± 5	141 ± 8	26.4 ± 1.4	2.46 ± 0.17	0
$AGES$ $J114039+195455$	11 : 40 : 39.0	0.7	19 : 54 : 55	11	7839 ± 3	186 ± 6	214 ± 10	6.7 ± 0.6	0.83 ± 0.09	0
$AGES$ $J114113+193240$	11 : 41 : 13.6	1.0	19 : 32 : 40	14	10011 ± 7	260 ± 14	291 ± 20	3.4 ± 0.6	0.50 ± 0.10	1
$AGES$ $J114118+200829$	11 : 41 : 18.0	0.7	20 : 08 : 29	11	14616 ± 4	156 ± 7	186 ± 11	5.8 ± 0.6	0.76 ± 0.08	0
$AGES$ $J114129+200550$	11 : 41 : 29.5	1.1	20 : 05 : 50	21	14591 ± 8	146 ± 16	194 ± 25	3.0 ± 0.5	0.33 ± 0.07	1
$AGES$ $J114131+201912$	11 : 41 : 31.5	0.9	20 : 19 : 12	18	3504 ± 9	23 ± 18	90 ± 26	4.6 ± 0.7	0.11 ± 0.05	1
$AGES$ $J114143+193536$	11 : 41 : 43.4	0.7	19 : 35 : 36	10	16787 ± 4	125 ± 8	157 ± 13	6.1 ± 0.7	0.58 ± 0.08	0
$AGES$ $J114148+194538$	11 : 41 : 48.0	0.7	19 : 45 : 38	10	7811 ± 6	138 ± 12	201 ± 18	6.0 ± 0.7	0.73 ± 0.09	0
$AGES$ $J114204+194536$	11 : 42 : 04.0	0.7	19 : 45 : 36	10	11059 ± 7	172 ± 15	210 ± 22	3.4 ± 0.6	0.35 ± 0.08	1
$AGES$ $J114209+201924$	11 : 42 : 09.3	0.7	20 : 19 : 24	10	5764 ± 5	319 ± 9	337 ± 14	5.9 ± 0.9	1.25 ± 0.18	0
$AGES$ $J114211+195827$	11 : 42 : 11.7	0.7	19 : 58 : 27	11	7774 ± 6	145 ± 12	246 ± 18	6.8 ± 0.6	0.88 ± 0.09	0
$AGES$ $J114216+200302$	11 : 42 : 16.0	1.5	20 : 03 : 02	19	6087 ± 5	112 ± 9	173 ± 14	6.7 ± 0.6	0.74 ± 0.08	0
$AGES$ $J114224+200710$	11 : 42 : 24.4	0.7	20 : 07 : 10	10	5979 ± 2	334 ± 3	353 ± 5	17.8 ± 1.0	4.30 ± 0.20	0
$AGES$ $J114239+201150$	11 : 42 : 39.6	0.8	20 : 11 : 50	10	5993 ± 8	169 ± 16	263 ± 23	4.6 ± 0.6	0.56 ± 0.08	0
$AGES$ $J114243+200143$	11 : 42 : 43.8	0.7	20 : 01 : 43	11	6338 ± 3	300 ± 6	307 ± 10	3.0 ± 0.5	0.46 ± 0.08	0
$AGES$ $J114255+195734$	11 : 42 : 55.9	0.7	19 : 57 : 34	10	7264 ± 7	186 ± 13	292 ± 20	7.5 ± 0.7	1.17 ± 0.11	0
$AGES$ $J114308+194210$	11 : 43 : 08.1	0.7	19 : 42 : 10	10	12952 ± 5	313 ± 10	371 ± 15	5.9 ± 0.6	1.32 ± 0.11	0
$AGES$ $J114311+200032$	11 : 43 : 11.8	0.7	20 : 00 : 32	11	7085 ± 7	65 ± 14	112 ± 21	4.2 ± 0.6	0.25 ± 0.06	2
$AGES$ $J114312+193655$	11 : 43 : 12.0	0.7	19 : 36 : 55	10	6247 ± 4	56 ± 8	93 ± 12	7.2 ± 0.7	0.36 ± 0.06	0
$AGES$ $J114331+193747$	11 : 43 : 31.6	0.7	19 : 37 : 47	10	13131 ± 4	274 ± 9	341 ± 13	8.2 ± 0.6	1.97 ± 0.13	0
$AGES$ $J114347+195820$	11 : 43 : 47.1	0.7	19 : 58 : 20	10	6904 ± 8	165 ± 16	547 ± 25	13.2 ± 0.8	2.65 ± 0.15	2
$AGES$ $J114358+200430$	11 : 43 : 58.5	0.7	20 : 04 : 30	10	7372 ± 2	258 ± 4	273 ± 6	12.3 ± 0.9	2.53 ± 0.16	0
$AGES$ $J114402+202313$	11 : 44 : 02.5	0.8	20 : 23 : 13	11	11843 ± 6	243 ± 11	274 ± 17	6.4 ± 1.0	0.72 ± 0.13	0
$AGES$ $J114416+201309$	11 : 44 : 16.4	0.8	20 : 13 : 09	12	6370 ± 6	302 ± 12	325 ± 18	3.3 ± 0.6	0.55 ± 0.10	0
$AGES$ $J114435+192841$	11 : 44 : 35.6	0.7	19 : 28 : 41	10	2765 ± 2	133 ± 3	144 ± 5	8.9 ± 0.7	1.05 ± 0.10	0
$AGES$ $J114447+200737$	11 : 44 : 47.7	0.7	20 : 07 : 37	11	6583 ± 3	392 ± 6	408 ± 9	5.1 ± 0.6	0.67 ± 0.08	0
$AGES$ $J114451+192723$	11 : 44 : 51.8	0.7	19 : 27 : 23	10	5478 ± 8	374 ± 15	456 ± 23	5.2 ± 0.7	1.25 ± 0.13	0
$AGES$ $J114452+194635$	11 : 44 : 52.9	0.7	19 : 46 : 35	10	8225 ± 8	261 ± 16	425 ± 25	8.6 ± 0.8	1.46 ± 0.14	0
$AGES$ $J114503+195832$	11 : 45 : 03.2	0.7	19 : 58 : 32	10	5091 ± 2	465 ± 4	494 ± 6	18.8 ± 1.1	6.37 ± 0.26	0
$AGES$ $J114508+200837$	11 : 45 : 08.5	0.7	20 : 08 : 37	11	3724 ± 2	74 ± 5	95 ± 7	9.6 ± 0.8	0.62 ± 0.08	0
$AGES$ $J114543+200147$	11 : 45 : 43.5	0.7	20 : 01 : 47	10	5322 ± 2	45 ± 4	80 ± 6	38.0 ± 2.0	1.56 ± 0.16	0
$AGES$ $J114545+194210$	11 : 45 : 45.9	0.8	19 : 42 : 10	12	6182 ± 7	154 ± 14	183 ± 21	3.1 ± 0.6	0.33 ± 0.08	1
$AGES$ $J114612+202403$	11 : 46 : 12.4	0.7	20 : 24 : 03	11	7026 ± 3	595 ± 7	610 ± 10	9.4 ± 1.2	2.39 ± 0.24	2
$AGES$ $J114625+193024$	11 : 46 : 25.5	0.7	19 : 30 : 24	10	2189 ± 3	103 ± 5	121 ± 8	6.0 ± 0.6	0.54 ± 0.07	0
$AGES$ $J114638+194854$	11 : 46 : 38.1	0.9	19 : 48 : 54	14	5416 ± 9	97 ± 19	149 ± 28	2.7 ± 0.5	0.21 ± 0.06	1
$AGES$ $J114646+191906$	11 : 46 : 46.8	0.7	19 : 19 : 06	11	14644 ± 9	173 ± 18	277 ± 28	7.2 ± 1.0	0.96 ± 0.14	0
$AGES$ $J114724+192324$	11 : 47 : 24.1	0.7	19 : 23 : 24	10	5854 ± 4	159 ± 7	175 ± 11	4.8 ± 0.6	0.52 ± 0.09	0
$AGES$ $J114727+194906$	11 : 47 : 27.4	0.8	19 : 49 : 06	11	5869 ± 7	60 ± 15	99 ± 22	3.6 ± 0.6	0.19 ± 0.06	1
$AGES$ $J114730+195353$	11 : 47 : 30.0	0.8	19 : 53 : 53	14	5759 ± 5	261 ± 11	282 ± 16	3.7 ± 0.6	0.41 ± 0.08	1
$AGES$ $J114739+195621$	11 : 47 : 39.7	0.7	19 : 56 : 21	10	6173 ± 2	386 ± 4	396 ± 6	7.1 ± 0.7	1.29 ± 0.12	0
$AGES$ $J114739+200924$	11 : 47 : 39.2	0.7	20 : 09 : 24	10	5316 ± 5	124 ± 11	156 ± 16	3.7 ± 0.5	0.37 ± 0.07	0
$AGES$ $J114809+192109$	11 : 48 : 09.1	2.4	19 : 21 : 09	18	11252 ± 5	171 ± 9	179 ± 14	3.3 ± 0.8	0.34 ± 0.10	1
$AGES$ $J114823+194244$	11 : 48 : 23.1	0.7	19 : 42 : 44	10	5079 ± 7	82 ± 14	155 ± 21	4.5 ± 0.5	0.25 ± 0.05	1
$AGES$ $J114824+202331$	11 : 48 : 24.3	0.9	20 : 23 : 31	17	6750 ± 8	80 ± 15	143 ± 23	9.8 ± 1.4	0.64 ± 0.14	0
$AGES$ $J114829+194529$	11 : 48 : 29.3	1.1	19 : 45 : 29	11	5586 ± 4	121 ± 8	144 ± 13	5.7 ± 0.8	0.41 ± 0.08	0
$AGES$ $J114956+192840$	11 : 49 : 56.7	0.8	19 : 28 : 40	11	6139 ± 4	67 ± 7	82 ± 11	3.9 ± 0.5	0.23 ± 0.05	1
$AGES$ $J115030+200505$	11 : 50 : 30.0	0.8	20 : 05 : 05	11	6021 ± 7	161 ± 14	185 ± 21	2.9 ± 0.6	0.27 ± 0.08	1
$AGES$ $J115034+194301$	11 : 50 : 34.4	0.7	19 : 43 : 01	10	6633 ± 7	88 ± 15	162 ± 22	5.2 ± 0.7	0.38 ± 0.07	0
$AGES$ $J115052+193102$	11 : 50 : 52.7	0.7	19 : 31 : 02	11	11829 ± 8	270 ± 16	336 ± 24	3.7 ± 0.5	0.67 ± 0.09	0
$AGES$ $J115101+193728$	11 : 51 : 01.0	0.7	19 : 37 : 28	11	11626 ± 4	247 ± 8	268 ± 12	4.3 ± 0.5	0.53 ± 0.08	0
$AGES$ $J115101+202355$	11 : 51 : 01.8	0.7	20 : 23 : 55	10	6453 ± 2	269 ± 4	284 ± 5	21.8 ± 1.5	3.45 ± 0.24	0
$AGES$ $J115120+192931$	11 : 51 : 20.4	0.8	19 : 29 : 31	10	11971 ± 4	201 ± 9	226 ± 13	4.2 ± 0.5	0.42 ± 0.07	0
$AGES$ $J115147+192057$	11 : 51 : 47.4	0.7	19 : 20 : 57	11	6931 ± 3	343 ± 6	354 ± 9	5.1 ± 0.7	0.61 ± 0.09	2
$AGES$ $J115150+194720$	11 : 51 : 50.7	1.0	19 : 47 : 20	14	6361 ± 4	102 ± 9	119 ± 13	3.2 ± 0.5	0.23 ± 0.06	1
$AGES$ $J115156+193838$	11 : 51 : 56.1	0.7	19 : 38 : 38	10	6060 ± 2	187 ± 5	212 ± 7	11.7 ± 0.8	1.58 ± 0.12	0
$AGES$ $J115202+193423$	11 : 52 : 02.3	0.7	19 : 34 : 23	10	11989 ± 5	163 ± 10	186 ± 15	3.3 ± 0.5	0.33 ± 0.07	0
$AGES$ $J115223+201943$	11 : 52 : 23.5	0.7	20 : 19 : 43	12	6491 ± 5	128 ± 10	180 ± 15	8.6 ± 0.9	0.95 ± 0.12	0
$AGES$ $J115227+200821$	11 : 52 : 27.9	0.7	20 : 08 : 21	10	16085 ± 7	140 ± 14	167 ± 20	3.2 ± 0.6	0.35 ± 0.08	1
$AGES$ $J115250+201423$	11 : 52 : 50.5	0.7	20 : 14 : 23	10	14678 ± 3	186 ± 6	218 ± 10	10.2 ± 0.9	1.64 ± 0.14	0
$AGES$ $J115318+200622$	11 : 53 : 18.0	0.7	20 : 06 : 22	10	6215 ± 3	112 ± 5	163 ± 8	19.7 ± 1.1	2.01 ± 0.14	0
$AGES$ $J115349+194505$	11 : 53 : 49.8	0.7	19 : 45 : 05	10	12047 ± 6	447 ± 12	493 ± 17	6.0 ± 0.8	1.28 ± 0.14	0
$AGES$ $J115356+201043$	11 : 53 : 56.2	0.8	20 : 10 : 43	11	15210 ± 4	228 ± 8	236 ± 11	3.7 ± 0.7	0.49 ± 0.11	$1-2$
$AGES$ $J115358+195734$	11 : 53 : 58.9	0.7	19 : 57 : 34	11	15336 ± 9	125 ± 17	193 ± 26	4.0 ± 0.6	0.43 ± 0.08	2
$AGES$ $J115414+200138$	11 : 54 : 14.1	0.7	20 : 01 : 38	11	6208 ± 3	225 ± 7	249 ± 10	10.0 ± 1.0	1.50 ± 0.16	0

Table 2. HI parameters for the 22 sources observed with Lwide and confirmed.

$HI-ID$	V $\mathrm{km\,s^{-1}}$	$W50$ $\mathrm{km\,s^{-1}}$	$W20$ $\mathrm{km\,s^{-1}}$	F_{tot} $\mathrm{Jy\ km\,s^{-1}}$	rms mJy
$AGES\ J113508+201210$	16144 ± 6	99 ± 12	128 ± 18	0.37 ± 0.08	0.77
$AGES\ J113524+200009$	9556 ± 7	303 ± 13	340 ± 20	0.40 ± 0.07	0.52
$AGES\ J113801+200106$	19086 ± 11	243 ± 22	372 ± 33	0.89 ± 0.12	0.80
$AGES\ J113835+195550$	13198 ± 5	286 ± 9	294 ± 14	0.52 ± 0.12	0.80
$AGES\ J113904+194129$	16917 ± 10	54 ± 19	113 ± 29	0.22 ± 0.07	0.70
$AGES\ J113926+194459$	17186 ± 7	167 ± 15	203 ± 22	0.45 ± 0.10	0.80
$AGES\ J113942+200817$	16915 ± 7	25 ± 14	87 ± 21	0.13 ± 0.05	0.80
$AGES\ J114113+193240$	10008 ± 9	256 ± 19	297 ± 28	0.45 ± 0.11	0.75
$AGES\ J114129+200550$	14584 ± 7	161 ± 14	190 ± 21	0.22 ± 0.06	0.54
$AGES\ J114131+201912$	3506 ± 6	68 ± 12	98 ± 17	0.22 ± 0.06	0.80
$AGES\ J114204+194536$	11066 ± 15	134 ± 30	225 ± 45	0.22 ± 0.07	0.55
$AGES\ J114545+194210$	6168 ± 10	147 ± 20	181 ± 30	0.26 ± 0.08	0.58
$AGES\ J114638+194854$	5421 ± 12	113 ± 23	184 ± 34	0.18 ± 0.06	0.55
$AGES\ J114727+194906$	5864 ± 7	86 ± 13	113 ± 19	0.19 ± 0.05	0.52
$AGES\ J114730+195353$	5765 ± 13	176 ± 26	287 ± 38	0.36 ± 0.08	0.52
$AGES\ J114809+192109$	11249 ± 9	71 ± 18	128 ± 26	0.18 ± 0.06	0.72
$AGES\ J114823+194244$	5078 ± 8	67 ± 16	102 ± 24	0.24 ± 0.08	0.75
$AGES\ J114956+192840$	6136 ± 4	76 ± 8	87 ± 11	0.09 ± 0.04	0.52
$AGES\ J115030+200505$	6022 ± 4	177 ± 8	247 ± 12	0.28 ± 0.02	0.60
$AGES\ J115150+194720$	6357 ± 4	104 ± 8	115 ± 12	0.25 ± 0.07	0.76
$AGES\ J115227+200821$	16091 ± 7	164 ± 14	211 ± 21	0.34 ± 0.07	0.56
$AGES\ J115356+201043$	15197 ± 5	228 ± 10	248 ± 14	0.47 ± 0.09	0.80

Table 3. List of optical counterparts for the 100 HI sources in A1367

$HI-ID$	$Optical-ID$	$R.A.$ (J.2000)	$Dec.$ (J.2000)	$Optical\ Velocity$ km s^{-1}
$AGES\ J113444+201217$	$MAPS-NGPO\_434\_0001768$	11 : 34 : 46.01	20 : 12 : 17.2	9652*
$AGES\ J113508+201210$	$SDSSJ113508.79+201216.1$	11 : 35 : 08.79	20 : 12 : 16.1	−−
$AGES\ J113523+201823$	$KUG1132+205$	11 : 35 : 23.13	20 : 18 : 42.4	10451
$AGES\ J113524+200009$	$MAPS-NGPO\_375\_1208433$	11 : 35 : 27.77	20 : 00 : 2.7	−−
$AGES\ J113544+195120$	$SDSSJ113544.31+195114.0$	11 : 35 : 44.31	19 : 51 : 14	−−
$AGES\ J113553+201308$	$KUG1133+204$	11 : 35 : 54.44	20 : 13 : 19.9	1097*
$AGES\ J113614+195910$	−−	−−	−−	−−
$AGES\ J113626+195102$	−−	−−	−−	−−
$AGES\ J113641+200622$	$MAPS-NGPO\_434\_0002451$	11 : 36 : 41.66	20 : 06 : 38.9	−−
$AGES\ J113653+200003$	$KUG1134+202A$	11 : 36 : 54.24	19 : 59 : 49.9	6630
$AGES\ J113657+195837$	$UGC06583$	11 : 36 : 54.40	19 : 58 : 15.0	6191
$AGES\ J113718+192129$	$KUG1134+196$	11 : 37 : 17.60	19 : 21 : 36.0	14370
$AGES\ J113736+200934$	$CGCG097-033$	11 : 37 : 36.00	20 : 09 : 49.0	7736
$AGES\ J113743+195559$	$SDSSJ113744.57+195556.7$	11 : 37 : 44.57	19 : 55 : 56.7	−−
	$SDSSJ113744.21+195616.2$	11 : 37 : 44.21	19 : 56 : 16.2	−−
	$SDSSJ113743.51+195555.4$	11 : 37 : 43.51	19 : 55 : 55.4	−−
$AGES\ J113801+200106$	$SDSSJ113804.47+200021.8$	11 : 38 : 04.47	20 : 00 : 21.8	−−
	$SDSSJ113804.46+200043.4$	11 : 38 : 04.46	20 : 00 : 43.4	−−
$AGES\ J113804+195146$	$2MASXJ11380386+1951420$	11 : 38 : 03.90	19 : 51 : 41.0	6196
$AGES\ J113804+201441$	$MAPS-NGPO\_434\_0002980$	11 : 38 : 00.73	20 : 14 : 32.3	−−
$AGES\ J113805+193250$	$2MASXJ11380463+1933020$	11 : 38 : 05.00	19 : 33 : 01.0	17891
$AGES\ J113828+195823$	$LSBCD571-03$	11 : 38 : 28.16	19 : 58 : 50.1	6981
$AGES\ J113835+195550$	$2MASXJ11383847+1954564$	11 : 38 : 38.49	19 : 54 : 56.7	−−
$AGES\ J113842+200527$	$SDSSJ113845.65+200511.4$	11 : 38 : 45.65	20 : 05 : 11.4	−−
$AGES\ J113844+200821$	$KUG1136+204$	11 : 38 : 45.26	20 : 08 : 24.1	3131*
$AGES\ J113850+193622$	$KUG1136+198$	11 : 38 : 51.00	19 : 36 : 04.0	6787
$AGES\ J113904+194129$	$SDSSJ113906.75+194135.1$	11 : 39 : 06.75	19 : 41 : 35.1	−−
$AGES\ J113910+193558$	$FGC1287$	11 : 39 : 10.95	19 : 35 : 06.0	6825
$AGES\ J113913+195915$	$MAPS-NGPO\_434\_0016203$	11 : 39 : 11.00	19 : 59 : 00.9	−−
$AGES\ J113922+193232$	$CGCG097-041$	11 : 39 : 24.50	19 : 32 : 04.0	6778
$AGES\ J113926+194459$	$KUG1136+200$	11 : 39 : 28.71	19 : 44 : 12.1	−−
$AGES\ J113930+191706$	$MAPS-NGPO\_434\_0045678$	11 : 39 : 31.78	19 : 17 : 24.9	−−
$AGES\ J113936+202020$	$2MASXJ11393700+2020039$	11 : 39 : 37.00	20 : 20 : 03.9	−−
$AGES\ J113939+193524$	$SDSSLSB$	11 : 39 : 40.17	19 : 35 : 20.0	−−
$AGES\ J113942+200817$	$SDSSJ113945.23+200806.9$	11 : 39 : 45.23	20 : 08 : 07.0	−−
$AGES\ J113945+195341$	$KUG1137+201A$	11 : 39 : 44.85	19 : 53 : 57.8	−−
$AGES\ J113947+195559$	$UGC06625$	11 : 39 : 47.60	19 : 55 : 60.0	10964
$AGES\ J113956+195955$	$KUG1137+202B$	11 : 39 : 57.20	20 : 00 : 13.0	10098
$AGES\ J114016+194715$	$[IBG2003]J114017+194718$	11 : 40 : 17.26	19 : 47 : 19.1	−−
$AGES\ J114027+192429$	$KUG1137+196$	11 : 40 : 26.15	19 : 24 : 51.9	3421
$AGES\ J114039+195455$	$[IBC2002]J114038+195437$	11 : 40 : 38.99	19 : 54 : 38.5	7784
$AGES\ J114113+193240$	$KUG1138+198$	11 : 41 : 13.43	19 : 32 : 21.7	10011
$AGES\ J114118+200829$	$KUG1138+204$	11 : 41 : 17.45	20 : 08 : 33.4	14500
$AGES\ J114129+200550$	$SDSSJ114130.18+200629.8$	11 : 41 : 30.18	20 : 06 : 29.8	−−
	$SDSSJ114129.01+200550.4$	11 : 41 : 29.01	20 : 05 : 50.4	−−
	$SDSSJ114129.74+200506.0$	11 : 41 : 29.74	20 : 05 : 06.0	−−
$AGES\ J114131+201912$	$SDSSJ114134.75+201917.9$	11 : 41 : 34.75	20 : 19 : 17.9	−−
	$SDSSJ114128.58+201803.8$	11 : 41 : 28.58	20 : 18 : 03.8	−−
$AGES\ J114143+193536$	$MAPS-NGPO\_434\_0037838$	11 : 41 : 43.22	19 : 35 : 26.2	−−
$AGES\ J114148+194538$	$[IBC2002]J114149+194605$	11 : 41 : 49.83	19 : 46 : 04.4	7789
$AGES\ J114204+194536$	$SDSSJ114205.74+194611.7$	11 : 42 : 05.74	19 : 46 : 11.7	−−
$AGES\ J114209+201924$	$NGC3821$	11 : 42 : 09.09	20 : 18 : 56.6	5788
$AGES\ J114211+195827$	$KUG1139+202$	11 : 42 : 14.77	19 : 58 : 35.2	7815
$AGES\ J114216+200302$	$KUG1139+203$	11 : 42 : 15.66	20 : 02 : 55.5	6102
$AGES\ J114224+200710$	$CGCG097-068$	11 : 42 : 24.48	20 : 07 : 09.9	5974
$AGES\ J114239+201150$	−−	−−	−−	−−
$AGES\ J114243+200143$	$CGCG097-072$	11 : 42 : 45.21	20 : 01 : 56.6	6332
$AGES\ J114255+195734$	$CGCG097-073$	11 : 42 : 56.46	19 : 57 : 58.4	7275
$AGES\ J114308+194210$	$KUG1140+199$	11 : 43 : 07.96	19 : 41 : 57.4	12988
$AGES\ J114311+200032$	$CGCG097-079$	11 : 43 : 13.32	20 : 00 : 17.5	7000
$AGES\ J114312+193655$	$[IBC2002]J114313+193645$	11 : 43 : 13.02	19 : 36 : 46.6	6121
$AGES\ J114331+193747$	$CGCG097-083$	11 : 43 : 31.22	19 : 37 : 40.6	13126
$AGES\ J114347+195820$	$UGC06697$	11 : 43 : 49.11	19 : 58 : 06.2	6725
$AGES\ J114358+200430$	$NGC3840$	11 : 43 : 59.01	20 : 04 : 37.3	7368
$AGES\ J114402+202313$	$2MASXJ11435706+2022383$	11 : 44 : 01.92	20 : 22 : 51.6	11962
$AGES\ J114416+201309$	$CGCG097-102$	11 : 44 : 17.22	20 : 13 : 23.9	6368
$AGES\ J114435+192841$	$MAPS-NGPO\_434\_0047286$	11 : 44 : 36.39	19 : 28 : 40.1	−−
$AGES\ J114447+200737$	$UGC06719$	11 : 44 : 47.12	20 : 07 : 30.2	6571
$AGES\ J114451+192723$	$NGC3859$	11 : 44 : 52.24	19 : 27 : 15.2	5468
$AGES\ J114452+194635$	$CGCG097-125$	11 : 44 : 54.85	19 : 46 : 34.9	8271
$AGES\ J114503+195832$	$NGC3861$	11 : 45 : 03.87	19 : 58 : 25.1	5085
$AGES\ J114508+200837$	$[IBG2003]J114506+200849$	11 : 45 : 06.40	20 : 08 : 49.2	3822
$AGES\ J114543+200147$	$CGCG097-138$	11 : 45 : 44.67	20 : 01 : 51.6	5313
$AGES\ J114545+194210$	$[IBG2003]J114545+194130$	11 : 45 : 45.27	19 : 41 : 30.7	6123
$AGES\ J114612+202403$	$NGC3884$	11 : 46 : 12.19	20 : 23 : 29.9	6946
$AGES\ J114625+193024$	$SDSSJ114626.45+193011.9$	11 : 46 : 26.45	19 : 30 : 11.9	−−
$AGES\ J114638+194854$	$SDSSJ114636.47+194834.1$	11 : 46 : 36.47	19 : 48 : 34.1	−−
	$SDSSJ114640.32+194820.8$	11 : 46 : 40.32	19 : 48 : 20.8	−−
$AGES\ J114646+191906$	$2MASXJ11464700+1919462$	11 : 46 : 47.03	19 : 19 : 46.2	−−
$AGES\ J114724+192324$	$MAPS-NGPO\_434\_0048296$	11 : 47 : 25.08	19 : 23 : 31.4	−−
$AGES\ J114727+194906$	$SDSSJ114730.39+194859.0$	11 : 47 : 30.39	19 : 48 : 59.0	−−
$AGES\ J114730+195353$	$2MASXJ11473099+1952201$	11 : 47 : 30.99	19 : 52 : 20.8	5778
$AGES\ J114739+195621$	$CGCG097-152$	11 : 47 : 39.35	19 : 56 : 22.0	6166
$AGES\ J114739+200924$	$SDSSJ114737.57+200900.6$	11 : 47 : 37.57	20 : 09 : 00.6	−−
$AGES\ J114809+192109$	−−	−−	−−	−−
$AGES\ J114823+194244$	$SDSSJ114825.21+194217.0$	11 : 48 : 25.21	19 : 42 : 17.0	−−
$AGES\ J114824+202331$	$LSBCD571-02$	11 : 48 : 26.40	20 : 23 : 19.0	6796
$AGES\ J114829+194529$	$MAPS-NGPO\_434\_0031444$	11 : 48 : 28.43	19 : 45 : 36.0	−−
$AGES\ J114956+192840$	$SDSSJ114956.75+192840.4$	11 : 49 : 56.76	19 : 28 : 40.4	−−
	$SDSSJ114956.93+192830.7$	11 : 49 : 56.93	19 : 28 : 30.7	−−
$AGES\ J115030+200505$	$MAPS-NGPO\_434\_0021239$	11 : 50 : 29.99	20 : 05 : 08.2	−−
$AGES\ J115034+194301$	$SDSSJ115033.61+194250.1$	11 : 50 : 33.61	19 : 42 : 50.1	−−
$AGES\ J115052+193102$	$KUG1148+197A$	11 : 50 : 52.48	19 : 31 : 10.8	−−
$AGES\ J115101+193728$	$2MASXJ11510128+1937311$	11 : 51 : 01.29	19 : 37 : 31.3	−−
$AGES\ J115101+202355$	$UGC06821$	11 : 51 : 01.12	20 : 23 : 57.3	6438
$AGES\ J115120+192931$	$KUG1148+197$	11 : 51 : 21.28	19 : 29 : 33.9	−−
$AGES\ J115147+192057$	$KUG1149+196$	11 : 51 : 48.37	19 : 21 : 29.3	6932

*: new optical redshift obtained in Winter 2007 using the Loiano 1.5 meter telescope.

Table 3. Continue.

$HI-ID$	$Optical-ID$	$R.A.$ (J.2000)	$Dec.$ (J.2000)	$Optical\ Velocity$ $\mathrm{km\,s^{-1}}$
$AGES\ J115150+194720$	$SDSSJ115150.33+194702.6$	11 : 51 : 50.33	19 : 47 : 02.7	$--$
	$SDSSJ115150.87+194613.2$	11 : 51 : 50.87	19 : 46 : 13.2	$--$
$AGES\ J115156+193838$	$KUG1149+199$	11 : 51 : 55.65	19 : 38 : 45.4	6134*
$AGES\ J115202+193423$	$SDSSJ115203.86+193425.5$	11 : 52 : 03.86	19 : 34 : 25.5	$--$
$AGES\ J115223+201943$	$KUG1149+206$	11 : 52 : 24.44	20 : 19 : 28.8	6491
$AGES\ J115227+200821$	$2MASXJ11522887+2007597$	11 : 52 : 28.85	20 : 07 : 59.5	$--$
$AGES\ J115250+201423$	$KUG1150+205$	11 : 52 : 51.04	20 : 14 : 21.9	14679
$AGES\ J115318+200622$	$KUG1150+203$	11 : 53 : 18.28	20 : 06 : 26.6	6061*
$AGES\ J115349+194505$	$CGCG097-176$	11 : 53 : 50.34	19 : 45 : 01.5	12005
$AGES\ J115356+201043$	$MAPS-NGPO\_376\_4233155$	11 : 53 : 55.94	20 : 10 : 55.6	$--$
$AGES\ J115358+195734$	$KUG1151+202$	11 : 53 : 59.89	19 : 57 : 27.1	15489
$AGES\ J115414+200138$	$KUG1151+203$	11 : 54 : 13.94	20 : 01 : 39.0	6187

*: new optical redshift obtained in Winter 2007 using the Loiano 1.5 meter telescope.

Table 4. SDSS-Blue galaxies undetected in HI.

$R.A.$ (J.2000)	$Dec.$ (J.2000)	$Name.$	u mag	g mag	r mag	i mag	z mag	$g-i$ mag	V $\mathrm{km\,s^{-1}}$	$R_{iso}(r)$ $arcsec$	$R_{iso}(H\alpha)$ $arcsec$
11 : 42 : 18.12	+29 : 50 : 15.9	$KUG1139+201$	17.15	15.88	15.40	15.12	14.98	0.76	6476	11.6	3.0
11 : 43 : 47.76	+20 : 21 : 48.0	$KUG1141+206A$	17.59	16.12	15.66	15.43	15.25	0.71	6722	15.1	6.8
11 : 43 : 48.90	+20 : 14 : 54.0	$KUG1141+205$	17.33	16.35	15.90	15.78	15.60	0.57	6103	8.0	4.8
11 : 43 : 49.88	+19 : 58 : 34.8	$CGCG97-087N$	18.04	16.78	16.49	16.18	16.01	0.60	7542	19.0	6.0
11 : 43 : 58.23	+20 : 11 : 07.9	$CGCG97-092$	16.46	15.39	14.95	14.70	14.52	0.70	6487	$--$	$--$
11 : 44 : 01.94	+19 : 47 : 03.9	$CGCG97-093$	16.37	15.47	15.18	15.05	14.98	0.42	4909	24.0	9.1
11 : 44 : 13.90	+19 : 20 : 11.3	$MAPS-NGPO\_434\_0047177$	17.48	16.96	16.79	16.73	16.66	0.23	5852	10.3	8.6
11 : 44 : 54.56	+20 : 01 : 01.4	$KUG1142+202A$	17.85	16.65	16.20	15.93	15.73	0.73	7646	10.8	3.2